

Quantum Compiler for Classical Dynamical Systems

Dimitrios Giannakis

*Department of Mathematics and Center for Atmosphere Ocean Science,
Courant Institute of Mathematical Sciences, New York University, New York, NY 10012, USA*

Abbas Ourmazd

Department of Physics, University of Wisconsin–Milwaukee, Milwaukee, WI 53211, USA

Jörg Schumacher

*Institut für Thermo- und Fluidodynamik, Technische Universität Ilmenau, D-98684 Ilmenau, Germany and
Tandon School of Engineering, New York University, New York, NY 11201, USA*

Joanna Slawinska

*Finnish Center for Artificial Intelligence, Department of Computer Science,
University of Helsinki, FI-00014 Helsinki, Finland*

(Dated: July 9, 2022)

We present a framework for simulating measure-preserving, ergodic dynamical systems on a quantum computer. Our approach is based on a quantum feature map representing classical states by density operators (quantum states) on a reproducing kernel Hilbert space (RKHS) \mathcal{H} of functions on classical state space. Simultaneously, a mapping is employed from classical observables into self-adjoint operators on \mathcal{H} such that quantum mechanical expectation values are consistent with pointwise function evaluation. Quantum states and observables on \mathcal{H} evolve under the action of a unitary group of Koopman operators in a compatible manner with classical dynamical evolution. To achieve quantum parallelism, the state of the quantum system is projected onto a finite-rank density operator on a 2^N -dimensional tensor product Hilbert space associated with N qubits. By employing discrete Fourier-Walsh transforms of spectral functions, the Hamiltonian of the finite-dimensional quantum system is decomposed into a sum of mutually commuting operators of pure tensor product form, implementable as an N -channel quantum circuit. In the special case of quasiperiodic dynamics, no interchannel communication is necessary. Circuits of higher complexity are required to simulate chaotic dynamics. The output of the quantum compiler is a stochastic simulator of the evolution of classical observables, realized through projective quantum measurements. Numerical examples, including a quantum circuit implementation using the Qiskit software development kit, demonstrate the consistency of the quantum compiler for simple dynamical systems.

I. INTRODUCTION

Ever since a seminal paper of Feynman in 1982 [1], the problem of identifying physical systems that can faithfully and efficiently simulate large classes of other systems (performing, in Feynman’s words, *universal computation*) has received considerable attention. Under the operating principle that nature is fundamentally quantum mechanical, and with the realization that simulating quantum systems by classical systems is exponentially hard, much effort has been focused on the design of universal simulators of quantum systems. Such efforts are based on the axioms of quantum mechanics, with gates connected in quantum circuits performing unitary (and thus reversible) transformations of quantum states [2–6]. Over the past decades, several numerically hard problems have been identified, for which quantum algorithms are significantly faster than their classical counterparts. One prominent example is the Grover search algorithm, which results in a polynomial speedup over classical search [7]. In a few cases, such as random sampling [8], quantum algorithms have achieved an exponential speedup, demonstrating so-called “quantum supremacy”.

Yet, at least at the level of effective theories, a great

variety of phenomena are well described by classical dynamical systems, generally formulated as systems of ordinary or partial differential equations. When simulating a classical system is exponentially hard, it is natural to ask whether simulation of a *classical* system by a quantum system is an exponentially “easy” problem, enabling a vast increase in the complexity and range of computationally amenable classical phenomena.

The possibility to simulate classical dynamical systems on a quantum computer has attracted significant attention. Already 20 years ago, for example, Benenti et al. [9] studied the sawtooth map generating rich and complex dynamics. The implementation of an Euler method to solve systems of coupled nonlinear ordinary differential equations (ODEs) was addressed in 2009 [10]. A framework for data assimilation of partially observed classical systems based on the von Neumann formalism of quantum dynamics and measurement was proposed in Ref. [11]. The simulation of classical Hamiltonian systems using a so-called Koopman-von Neumann approach was studied by Joseph [12] in 2020. This quantum computational framework was shown to be exponentially faster than a classical simulation, when the Hamiltonian is represented by a sparse matrix. Most recently, the

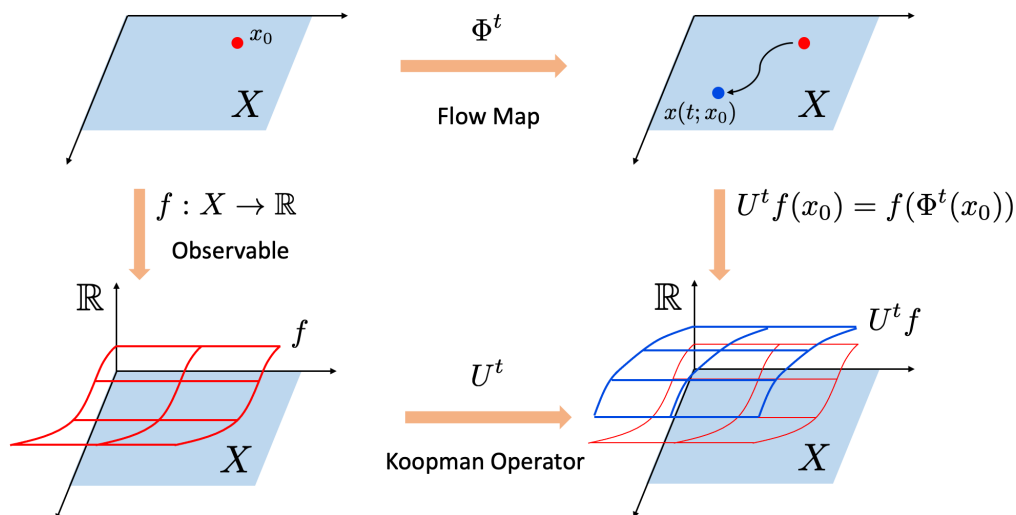


FIG. 1. Schematic of the relationship between the flow map Φ^t that advances the (nonlinear) dynamical system in a state space X in time and the linear Koopman operator U^t that advances observables f on X in an infinite-dimensional Hilbert space.

potential of quantum computing for fluid dynamics, in particular turbulence, was discussed in depth [13, 14]. Lubasch et al. [15] took a different path, modeling the one-dimensional Burgers equation by a variational quantum method, made possible by its correspondence with the nonlinear Schrödinger equation.

Here, we present a procedure for simulating a classical, measure-preserving, ergodic dynamical system by means of a finite-dimensional quantum mechanical system. This approach provides a data-driven route to combining classical and quantum algorithms, enabling the simulation of dynamical systems with otherwise intractably high-dimensional state spaces.

Our pipeline consists of two steps. (i) A dynamically consistent embedding of the classical state space X into the state space of an infinite-dimensional quantum system with a diagonalizable Hamiltonian. (ii) Eigenspace projection of the infinite-dimensional quantum system onto a finite-dimensional system, whose dynamics are representable by composition of basic commuting unitary transformations, realizable via quantum gates. The principal mathematical tools employed in this construction are the operator-theoretic representation of dynamical systems through Koopman and transfer operators [16, 17] and reproducing kernel Hilbert space (RKHS) theory [18, 19] for machine learning. The connection between the dynamical system and the Koopman operator is illustrated in Fig. 1, and will be discussed in greater detail in the next section. We refer to the resulting framework for encoding a classical dynamical system into a quantum system amenable to simulation by a quantum computer as a *quantum compiler*.

Here, we present theoretical results on the asymptotic consistency of the compiler, and illustrate its behavior by means of simple analytically solvable examples of dynamical systems. A notable aspect of our formulation is that

it will be primarily data-driven in view to applications to nonlinear systems. The quantum compiler receives as an input a time series of observations of the classical system, without requiring explicit knowledge of the equations of motion. As a result, the framework can naturally leverage recent developments in quantum machine learning [20–22].

The outline of this paper is as follows. In Section II, we lay out the mathematical framework underlying the quantum compiler. This is followed in Section III by a detailed description of the construction of the quantum compiler meeting these objectives in the context of measure-preserving, ergodic dynamical systems with pure point spectrum. In this setting, the dynamics of state variables and observables, including the construction of the basis of the underlying Hilbert space, can be treated analytically. Finally, in Section IV, we demonstrate the implementation of this example on the IBM quantum computing platform Qiskit [23, 24], and present numerical examples demonstrating the consistency of the quantum compiler in simple dynamical systems. Our primary conclusions are summarized in Section V. Technical results and derivations are collected in two appendices.

II. A ROUTE TO QUANTUM COMPILATION

In this section, we describe the main components of the quantum compiler. A diagrammatic representation, passing through classical, classical statistical, quantum mechanical, and quantum computational levels of description is displayed in Fig. 2. This diagram places the steps for states and observables side-by-side for comparison. In the following subsections, we discuss the individual horizontal and vertical connections (which are maps) in the four levels of this diagram.

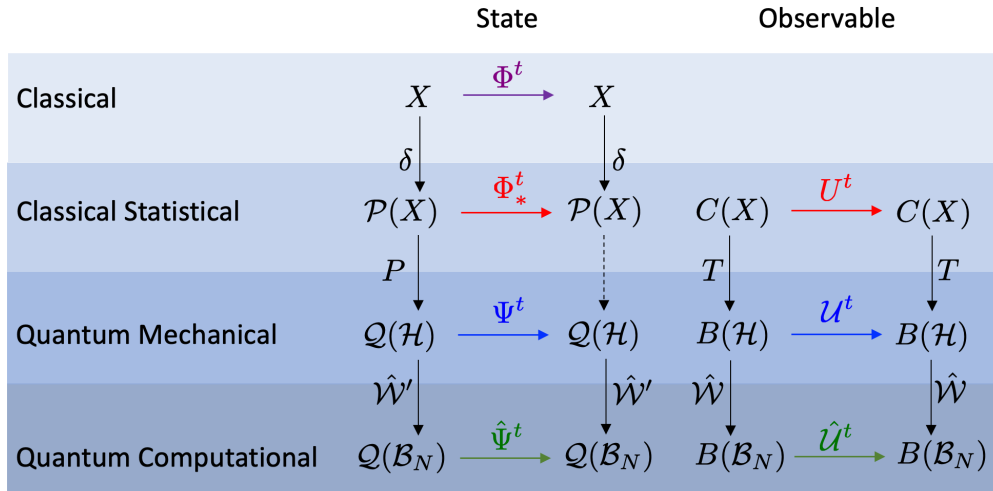


FIG. 2. Different representations of states and observables of a classical dynamical system and their relationship with the quantum computing model. Horizontal arrows represent the maps at a given level of description. The vertical arrows correspond to maps that translate states (left-hand column) and observables (right-hand column) to the next level of description. A loop of solid line arrows gives a commutative diagram.

A. Classical and classical statistical levels

We consider a classical dynamical system on a compact Hausdorff space X , described by a measure-preserving ergodic dynamical flow map

$$\Phi^t : X \rightarrow X \quad \text{with } t \in \mathbb{R},$$

as indicated by the magenta arrow in the left-hand column of Fig. 2. The classical state space X is embedded into the space of Borel probability measures $\mathcal{P}(X)$ (i.e., the classical statistical space) by means of the map δ sending $x \in X$ to the Dirac measure δ_x supported at x . The dynamics on the classical statistical space is governed by the transfer operator

$$\Phi_*^t : \mathcal{P}(X) \rightarrow \mathcal{P}(X),$$

which is equivariant with the flow map Φ^t , i.e., $\Phi_*^t \circ \delta = \delta \circ \Phi^t$ (see the red arrow in the left-hand column). This leads to the commutative relationships in the top two rows of the left column in Fig. 2.

Associated with the dynamical system is a space of classical observables, which we take here to be the space of continuous, complex-valued functions on X , denoted $C(X)$. In this context, a simulator of the system can be described as a procedure which takes as an input an observable $f \in C(X)$ and an initial condition $x \in X$, and produces as an output a time series $\hat{f}_t(x)$ approximating the evolution $f(\Phi^t(x))$ of the observable under the dynamics. For instance, if Φ^t is the flow generated by a system of ordinary differential equations (ODEs) $\dot{x} = \vec{V}(x)$ on $X = \mathbb{R}^d$, a classical way of performing simulation is to construct a finite-difference approximation $\hat{\Phi}^t : X \rightarrow X$ of the dynamical flow based on a timestep

Δt (using interpolation to generate a continuous-time trajectory), and obtain $\hat{f}_t(x) = f(\hat{\Phi}^t(x))$ by evaluating the observable of interest f on the approximate trajectory. The scheme then converges in a limit of $\Delta t \rightarrow 0$ by standard results in ODE theory and numerical analysis. The red arrow in the right-hand column of Fig. 2 represents the evolution of the observable provided by the Koopman operator [25, 26], which is given by

$$U^t : C(X) \rightarrow C(X) \quad \text{with } U^t f = f \circ \Phi^t; \quad (1)$$

see also Fig. 1. Here, rather than employing a classical approximating system $\hat{\Phi}^t$, our goal is to perform simulation of Φ^t using a quantum mechanical system.

B. From classical statistical to quantum computational

The quantum compiler effecting the representation of the classical system by a quantum mechanical system employs the following three key spaces: (1) the classical state space X , (2) an infinite-dimensional reproducing kernel Hilbert space (RKHS) $\mathcal{H} \subset C(X)$, and (3) a finite-dimensional Hilbert space \mathcal{B}_N together with its associated quantum states (density operators) and algebra of linear operators, acting as quantum mechanical states and observables, respectively. Below, N represents the number of qubits, thus the dimension of \mathcal{B}_N is 2^N .

The original classical state and observable spaces, X and $C(X)$, are mapped into spaces of quantum states (i.e., trace-class, positive operators of unit trace) and bounded operators on \mathcal{B}_N , respectively. These spaces are denoted by $\mathcal{Q}(\mathcal{B}_N)$ and $B(\mathcal{B}_N)$, respectively; see the bottom of Fig. 2. The following maps (vertical arrows)

for states (left-hand column) and observables (right-hand column) transform the classical system into a quantum-computational one on \mathcal{B}_N represented by a finite number of N qubits:

- A map $\hat{Q} : X \rightarrow \mathcal{Q}(\mathcal{B}_N)$ from classical states (points) in X to quantum mechanical states on \mathcal{B}_N . By analogy with the feature maps in machine learning [27], the composite map $\hat{Q} = \hat{W}' \circ P \circ \delta$ will be referred as a quantum feature map. To arrive at \hat{Q} , the classical statistical space $\mathcal{P}(X)$ is first embedded into the quantum mechanical state space $\mathcal{Q}(\mathcal{H})$ associated with the \mathcal{H} through an RKHS-induced embedding $P : \mathcal{P}(X) \rightarrow \mathcal{Q}(\mathcal{H})$ (see (8)). The composite map $P \circ \delta$ thus describes an embedding from classical states in X to quantum states in $\mathcal{Q}(\mathcal{H})$. The mapping $\hat{W}' : \mathcal{Q}(\mathcal{H}) \rightarrow \mathcal{Q}(\mathcal{B}_N)$ is induced by a partial isometry $\hat{W} : \mathcal{H} \rightarrow \mathcal{B}_N$.
- A linear map $\hat{T} : C(X) \rightarrow B(\mathcal{B}_N)$ from classical observables in $C(X)$ to quantum mechanical observables in $B(\mathcal{B}_N)$. Note that $\hat{T} = \hat{W} \circ T$. Here, T is one-to-one on the real-valued functions in \mathcal{H} , and $T(f)$ is self-adjoint whenever f is real.

Next, we describe the maps governing the temporal evolution of states and observables, represented by horizontal arrows in Fig. 2:

- At the quantum mechanical level, states in $\mathcal{Q}(\mathcal{H})$ evolve under the operator Ψ^t (blue arrow in the left-hand column) induced by a unitary Heisenberg operator e^{tV} on \mathcal{H} . This evolution is generated by a skew-adjoint generator $V : \mathcal{H} \rightarrow \mathcal{H}$ possessing a discrete spectrum of eigenfrequencies approximating the (potentially continuous) spectrum of the Koopman group on $L^2(\mu)$. Due to this approximation, the portion of the diagram in the second and third rows may not commute (i.e., in general, $\Psi^t \circ \delta \neq \delta \circ \Phi_*^t$), but the approximation error vanishes in a suitable limit.
- The generator V is mapped to the self-adjoint Hamiltonian $\hat{H} : \mathcal{B}_N \rightarrow \mathcal{B}_N$ given by $\hat{H} = \hat{W}V\hat{W}^*/i$. This Hamiltonian is decomposable as a sum $\hat{H} = \sum_j \hat{H}_j$ of mutually-commuting operators $\hat{H}_j \in B(\mathcal{B}_N)$, each of which is of pure tensor product form, $\hat{H}_j = \bigotimes_{i=1}^N \hat{H}_{ij}$. The latter property enables quantum parallelism in the unitary evolution $\hat{\Psi}^t : \mathcal{Q}(\mathcal{B}_N) \rightarrow \mathcal{Q}(\mathcal{B}_N)$ on the quantum computational level induced by \hat{H} (see green arrow in the left-hand column of Fig. 2).
- The blue arrow on the quantum mechanical level represents the action of the Heisenberg evolution operator $U^t : B(\mathcal{H}) \rightarrow B(\mathcal{H})$ on the space $B(\mathcal{H})$ of bounded operators on the RKHS \mathcal{H} . Under the assumption that \mathcal{H} is invariant under the Koopman operator, U^t acts on $B(\mathcal{H})$ by conjugation with U^t , i.e., $U^t A = U^t A U^{t*}$.

- The corresponding Heisenberg evolution operator on the quantum computational level $\hat{U}^t : B(\mathcal{B}_N) \rightarrow B(\mathcal{B}_N)$ acting on quantum mechanical observables on the Hilbert space \mathcal{B}_N is represented by the green arrow at the bottom of the right-hand column. This operator is obtained by conjugation of U^t by the same partial isometry $\hat{W} : \mathcal{H} \rightarrow \mathcal{B}_N$ employed in the lower loop in the commutative diagram in Fig. 2, i.e., $\hat{U}^t = \hat{W}U^t = \hat{W}U^t\hat{W}^*$.

Given a classical initial condition $x \in X$, the quantum mechanical system constructed by the compiler makes probabilistic predictions $\hat{f}_t(x)$ of $f(\Phi^t(x))$ through quantum mechanical measurement of the observable $\hat{A}_f = \hat{T}f$ on the state $\hat{\Psi}^t(\hat{\rho}_x)$, where $\hat{\rho}_x = \hat{Q}(x)$. The expectation value of $\hat{f}_t(x)$ is then given by

$$\bar{f}_t(x) := \langle \hat{A}_f \rangle_{\hat{\rho}_x} \equiv \text{tr}(\hat{\Psi}^t(\hat{\rho}_x)\hat{A}_f) \quad (2)$$

In order for this scheme to be successful, we shall require that the following four conditions be satisfied:

1. *Dynamical consistency.* The predictions made by the quantum system via (2) should converge in a suitable asymptotic limit of infinite dimension of \mathcal{B}_N to the true classical evolution.

2. *Quantum parallelism.* To take advantage of exponential parallelism afforded by quantum entanglement, the Hilbert space \mathcal{B}_N must be decomposable as a tensor product $\mathcal{B}_N = \mathcal{B}^{\otimes N}$, where \mathcal{B} is the Hilbert space associated with a single qubit, and N the number of qubits. Typically, $\mathcal{B} = \mathbb{C}^2$. Importantly, the Hamiltonian \hat{H} should be compatible with this factorization.

3. *Measurement process.* The process of querying the system to obtain predictions should be expressible as a quantum mechanical measurement associated with a projection-valued measure (PVM), or positive operator-valued measure (POVM) [4, 28], induced by \hat{A}_f .

4. *Empirical constructibility.* The quantum compiler should be able to build the output system from a finite trajectory x_0, x_1, \dots, x_{M-1} of the system with $x_m = \Phi^{m \Delta t}(x_0)$, or an ensemble of shorter trajectories.

III. QUANTUM COMPILER FOR QUASIPERIODIC DYNAMICS

We now describe the conversion to the quantum computing model for the class of continuous, measure-preserving, ergodic flows with a pure point spectrum generated by finitely many eigenfrequencies. Every such system is topologically conjugate to an ergodic rotation on a d -dimensional torus, so we will set $X = \mathbb{T}^d$ without loss of generality. Using the notation $x = (\theta_1, \dots, \theta_d)$ to represent a point $x \in \mathbb{T}^d$, where $\theta_j \in [0, 2\pi)$ are canonical

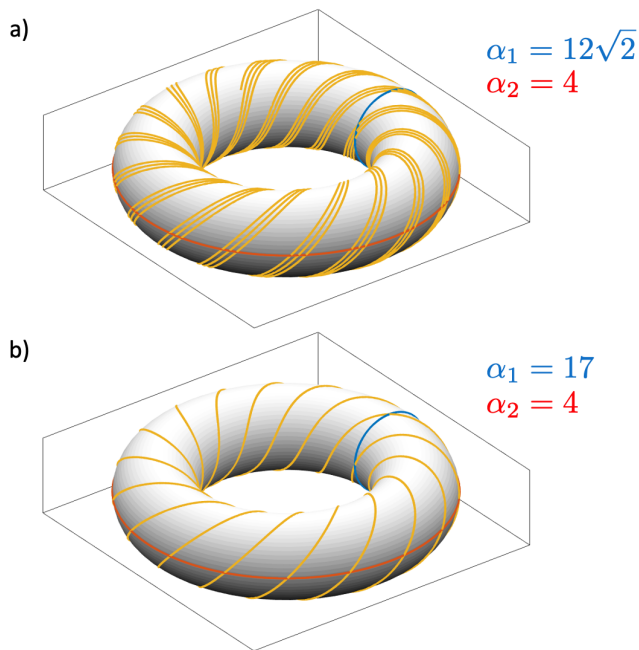


FIG. 3. Ergodic (a) and non-ergodic (b) linear flows on the two-dimensional torus \mathbb{T}^2 . In (a) the ratio of the frequency parameters α_1/α_2 is irrational, and the trajectory starts to fill the torus surface. In (b) the ratio of the frequencies is rational, and the trajectory is closed.

angle coordinates, the dynamics is described by the flow map

$$\Phi^t(x) = (\theta_1 + \alpha_1 t, \dots, \theta_d + \alpha_d t) \pmod{2\pi}, \quad (3)$$

where $\alpha_1, \dots, \alpha_d$ are positive, rationally independent (incommensurate) frequency parameters. This dynamical system is also known as a linear flow on a torus. Note that in dimension $d > 1$ the orbits $\Phi^t(x)$ of the dynamics do not close by incommensurability of the α_j , each forming a dense subset of the torus (i.e., a given orbit passes by any point in \mathbb{T}^d at an arbitrarily small distance). The case $d = 2$ is shown for two choices of α_j in Fig. 3, illustrating the difference between ergodic and non-ergodic dynamics. In dimension $d = 1$, the flow map corresponds to a harmonic oscillator on the circle, $\mathbb{T}^1 = S^1$, where each orbit is periodic and samples the whole space.

At every dimension d , this system is measure-preserving and ergodic for a probability measure μ given by a normalized Haar measure. The dynamics of classical observables $f : X \rightarrow \mathbb{C}$ is governed by the Koopman operator U^t , which acts by composition with the dynamical flow in accordance with (1). The Koopman operator [17, 29] acts as an isometry on the Banach space of continuous functions on X , i.e., $\|U^t f\|_{C(X)} = \|f\|_{C(X)}$, where $\|f\|_{C(X)} = \max_{x \in X} |f(x)|$ is the uniform norm. In addition, U^t lifts to a unitary operator on the Hilbert space $L^2(\mu)$ associated with the invariant measure. That is, using $\langle f, g \rangle_{L^2(\mu)} = \int_X f^* g d\mu$ to denote the $L^2(\mu)$ inner product, we have $\langle U^t f, U^t g \rangle_{L^2(\mu)} = \langle f, g \rangle_{L^2(\mu)}$ for all

$f, g \in L^2(\mu)$, which implies that $U^{t*} = U^{t-1}$. In particular, the collection $\{U^t : L^2(\mu) \rightarrow L^2(\mu)\}_{t \in \mathbb{R}}$ forms a strongly continuous unitary group under composition of operators; that is (i) $U^s \circ U^t = U^{s+t}$, (ii) $(U^t)^{-1} = U^{-t}$, and (iii) $\lim_{t \rightarrow 0} U^t f = f$ for all $s, t \in \mathbb{R}$ and $f \in L^2(\mu)$ (see again Fig. 1).

By Stone's theorem on one-parameter unitary evolution groups [30], the Koopman group on $L^2(\mu)$ has a skew-adjoint infinitesimal generator, i.e., an operator $V : D(V) \rightarrow L^2(\mu)$ defined on a dense subspace $D(V) \subset L^2(\mu)$ satisfying $V^* = -V$ and

$$Vf = \lim_{t \rightarrow 0} \frac{U^t f - f}{t}, \quad (4)$$

for all $f \in D(V)$. The generator gives the Koopman operator at any time t by exponentiation, $U^t = e^{tV}$. Modulo multiplication by $1/i$ to render it self-adjoint, it plays an analogous role to a quantum mechanical Hamiltonian generating the unitary Heisenberg evolution operators.

More generally, the torus rotation in (3) is a canonical representative of a wide class of continuous-time continuous dynamical systems on topological spaces with quasiperiodic dynamics generated by finitely many basic frequencies. This means that every such system can be transformed into an ergodic torus rotation of a suitable dimension by a homeomorphism (continuous, invertible map with invertible image), as noted above. By specializing, for now, to this class of systems (as opposed to a more general measure-preserving, ergodic flow), we gain two important properties:

- The dynamics has no mixing (chaotic) component. This implies that the spectrum of the Koopman operator for this system acting on $L^2(\mu)$, or a suitable RKHS as in what follows, is of “pure point” type, obviating complications arising from the presence of continuous spectrum as would be the case under mixing dynamics.

- The state space X is a smooth, closed manifold with the structure of a connected, abelian Lie group. The abelian group structure, in particular, renders this system amenable to analysis with tools from representation theory, including, for our purposes, the Fourier transform. Below, we use a d -dimensional vector $j = (j_1, \dots, j_d) \in \mathbb{Z}^d$ to represent a generic multi-index, and

$$\phi_j(x) = \varphi_{j_1}(\theta_1) \cdots \varphi_{j_d}(\theta_d), \quad \varphi_l(\theta) = e^{il\theta},$$

to represent the Fourier functions on \mathbb{T}^d . We also let $|j| := |j_1| + \dots + |j_d|$.

A. Choice of Hilbert space and representation of states

A central element of our approach to arrive at a quantum compiler meeting criteria set forth in Section II is to choose the Hilbert space for quantum computation as a

finite-dimensional subspace of an RKHS \mathcal{H} of complex-valued functions on the classical state space X . Intuitively, \mathcal{H} can be thought of as a (dense) subspace of $C(X)$ with additional Hilbert space structure. This structure is induced by a continuous, positive-definite kernel function $k : X \times X \rightarrow \mathbb{R}$, which has the properties that for every point $x \in X$ and function $f \in \mathcal{H}$ (i) the kernel section $k_x := k(x, \cdot)$ lies in \mathcal{H} ; and (ii) pointwise evaluation can be accomplished by the inner product

$$f(x) = \langle k_x, f \rangle_{\mathcal{H}}. \quad (5)$$

The latter is known as the reproducing property, and underlies the many useful properties of RKHSs for tasks such as function approximation and learning. Note, in particular, that L^2 spaces, which are more commonly employed in Koopman operator theory and techniques for measure-preserving dynamical systems, do not have a property analogous to (5). In fact, pointwise evaluation is not even defined for the $L^2(\mu)$ Hilbert space on \mathbb{T}^d . See Refs. [18, 19, 31] for detailed expositions on RKHS theory.

For our purposes, a key property that the RKHS structure of \mathcal{H} endows is the *feature map*, which is the continuous map $F : X \rightarrow \mathcal{H}$ mapping classical state $x \in X$ to the RKHS function

$$F(x) = k_x. \quad (6)$$

We will choose the kernel k to be *characteristic*, which implies that F is an injective map, and the functions $\{F(x) \in \mathcal{H} : x \in X\}$ are all linearly independent. It is then natural to think of the normalized feature vectors

$$\xi_x := \frac{k_x}{\|k_x\|_{\mathcal{H}}} = \frac{k_x}{\sqrt{k(x, x)}}$$

as “wavefunctions” corresponding to classical states $x \in X$.

We can generalize this idea by associating every such wavefunction ξ_x with the pure quantum state $\rho_x = \langle \xi_x, \cdot \rangle_{\mathcal{H}} \xi_x$. The mapping $Q : X \rightarrow \mathcal{Q}(\mathcal{H})$ with

$$Q(x) = \rho_x \quad (7)$$

then describes an embedding of the classical state space X into quantum mechanical states in $\mathcal{Q}(\mathcal{H})$. In particular, there is no loss of information in representing $x \in X$ by $\rho_x \in \mathcal{Q}(\mathcal{H})$. It should be noted that the quantum feature map (7) can be understood as the composition $Q = P \circ \delta$, where $\delta : X \rightarrow \mathcal{P}(X)$ maps classical state $x \in X$ to the Dirac probability measure $\delta_x \in \mathcal{P}(X)$, and $P : \mathcal{P}(X) \rightarrow \mathcal{Q}(\mathcal{H})$ is a map from classical probability measures on X to quantum states on \mathcal{H} , such that

$$P(p) = \int_X \rho_x dp(x). \quad (8)$$

See the left-hand column of Fig. 2 and Ref. [32] for further details on the properties of P .

We now describe the construction and properties of the RKHS \mathcal{H} appropriate for the torus $X = \mathbb{T}^d$. Given parameters $p > 0$ and $\tau > 0$, we start by defining the functions $|\cdot|_p : \mathbb{Z}^d \rightarrow \mathbb{R}_+$ and $\psi_j \in C(X)$ by

$$|j|_p := |j_1|^p + \dots + |j_d|^p, \quad \psi_j := e^{-\tau|j|_p/2} \phi_j.$$

We then construct a kernel $k : X \times X \rightarrow \mathbb{R}_+$ from the series

$$k(x, x') = \sum_{j \in \mathbb{Z}^d} \psi_j^*(x) \psi_j(x'), \quad (9)$$

where the sum over j converges uniformly on $X \times X$ to a smooth function. Intuitively, τ can be thought of as a “locality” parameter for the kernel, meaning that as τ decreases $k(x, x')$ becomes increasingly concentrated near $x = x'$, approaching a δ -function as $\tau \rightarrow 0$.

An important property of the kernel that holds for any $\tau > 0$ is that it is translation-invariant on the abelian group \mathbb{T}^d . That is, using additive notation to represent the binary group operation on \mathbb{T}^d , we have

$$k(x + y, x' + y) = k(x, x'), \quad \forall x, x', y \in \mathbb{T}^d. \quad (10)$$

In particular, setting $y = \Phi^t(e)$, where e is the identity element of \mathbb{T}^d , and noticing that the dynamical flow from (3) satisfies $\Phi^t(x) = x + \Phi^t(e)$, we deduce the dynamical invariance property.

$$k(\Phi^t(x), \Phi^t(x')) = k(x, x'), \quad \forall x, x' \in X, \quad \forall t \in \mathbb{R}.$$

For later convenience, we set

$$\kappa = k(x, x) = \sum_{j \in \mathbb{Z}^d} e^{-\tau|j|_p},$$

where this definition is independent of the point $x \in X$ by (10).

In Ref. [32] it was shown that for every $p > 0$ and $\tau > 0$, the kernel k in (9) is a strictly positive-definite, characteristic kernel on \mathbb{T}^d , so there is an associated RKHS \mathcal{H} with injective classical and quantum feature maps as described above. One can verify that the collection $\{\psi_j : j \in \mathbb{Z}^d\}$ forms an orthonormal basis of \mathcal{H} , consisting of scaled Fourier functions, so every observable $f \in \mathcal{H}$ admits the expansion

$$f = \sum_{j \in \mathbb{Z}^d} \tilde{f}_j \psi_j = \sum_{j \in \mathbb{Z}^d} \tilde{f}_j e^{-\tau|j|_p/2} \phi_j,$$

where the sum over j converges in \mathcal{H} norm. The above manifests the fact that \mathcal{H} contains continuous functions with exponentially decaying Fourier coefficients, implying in turn that every element of \mathcal{H} is a smooth function in $C^\infty(X)$.

It was also shown that for p lying in the open interval $(0, 1)$, the associated space \mathcal{H} acquires an important special property (which is not shared by generic RKHSs), namely it becomes an abelian, unital, Banach *-algebra under pointwise multiplication of functions. Specifically, this means that:

1. \mathcal{H} is closed under pointwise multiplication of functions, i.e., the function $h : X \rightarrow \mathbb{C}$ with $h(x) = f(x)g(x)$ lies in \mathcal{H} whenever f and g lie in \mathcal{H} . Thus, \mathcal{H} is an algebra, and is clearly abelian since $fg = gf$.

2. \mathcal{H} is equipped with an antilinear involution operation $*$: $\mathcal{H} \rightarrow \mathcal{H}$ given by complex conjugation of functions, i.e. $(f^*)(x) = f(x)^*$. Thus, \mathcal{H} is also a $*$ -algebra.

3. There exists a constant $C > 0$ such that for every $f, g \in \mathcal{H}$ the relationships

$$\|fg\|_{\mathcal{H}} \leq C\|f\|_{\mathcal{H}}\|g\|_{\mathcal{H}}, \quad \|f^*\|_{\mathcal{H}} = \|f\|_{\mathcal{H}}, \quad (11)$$

hold. Thus, \mathcal{H} is a Banach $*$ -algebra.

4. The function $1_X : X \rightarrow \mathbb{C}$ equal everywhere to 1 lies in \mathcal{H} and satisfies $1_X f = f$ for all $f \in \mathcal{H}$. Thus, finally \mathcal{H} is also unital.

In Ref. [32], the space \mathcal{H} was referred to as a reproducing kernel Hilbert algebra (RKHA) as it enjoys the properties of both RKHSs and Banach algebras. In particular, a distinguishing aspect of \mathcal{H} is that it simultaneously has Hilbert space structure (as $L^2(\mu)$) and Banach $*$ -algebra structure (as $C(X)$), while also allowing pointwise evaluation by continuous functionals (the reproducing property in (5)). Table I summarizes the properties of functions spaces on \mathbb{T}^d employed in this work. In what follows, we shall let \mathcal{H}_{sa} denote the set of self-adjoint elements of \mathcal{H} , i.e., the elements $f \in \mathcal{H}$ satisfying $f^* = f$. Since the $*$ operation of \mathcal{H} corresponds to complex conjugation of functions, it follows that \mathcal{H}_{sa} contains the real-valued functions in \mathcal{H} . Note that if $f = \sum_{j \in \mathbb{Z}^d} \tilde{f}_j \psi_j$ is an element of \mathcal{H}_{sa} , then its expansion coefficients in the ψ_j basis satisfy $\tilde{f}_j^* = \tilde{f}_{-j}$.

Next, we state a product formula for the orthonormal basis functions ψ_j , which follows directly from their definition, viz.

$$\begin{aligned} \psi_j \psi_l &= c_{jl} \psi_{j+l} \quad \text{with} \\ c_{jl} &= \exp\left(-\tau \frac{|j|_p + |l|_p - |j+l|_p}{2}\right). \end{aligned} \quad (12)$$

In the above, we interpret the coefficients c_{jl} as ‘‘structure constants’’ of the RKHA \mathcal{H} . Figure 4 displays representative matrices formed by the c_{jl} in dimension $d = 1$ and 2 for $p = 1/4$ and $\tau = 1/4$.

In the special case $d = 1$, we will let $\mathcal{H}^{(1)}$ be the RKHA on the circle $S^1 \equiv \mathbb{T}^1$ constructed as above. We denote the reproducing kernel of $\mathcal{H}^{(1)}$ by $k^{(1)}$, and let $\psi_j^{(1)}$, $j \in \mathbb{Z}$, be the corresponding orthonormal basis functions with $\psi_j^{(1)}(\theta) = e^{-|j|_p \tau/2} \varphi_j(\theta)$. It then follows that \mathcal{H} admits the tensor product factorization

$$\mathcal{H} = \bigotimes_{i=1}^d \mathcal{H}^{(1)},$$

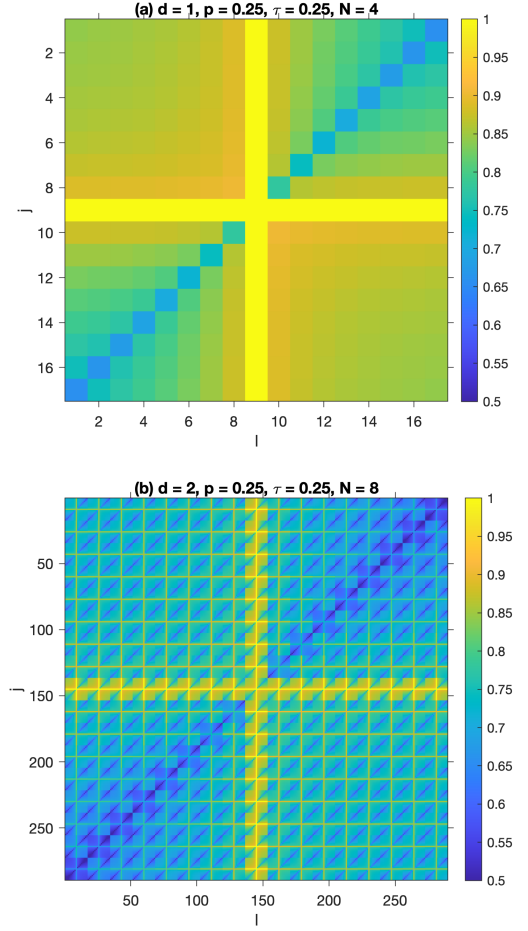


FIG. 4. Structure constant matrices (c_{jl}) for RKHAs on the circle ($d = 1$; a) and 2-torus ($d = 2$; b). In both cases, we use the parameter values $p = 1/4$ and $\tau = 1/4$. In (a), we consider indices in the range $-2^{N-1} \leq j, l \leq 2^{N-1}$ for $N = 4$. In (b), the multi-indices $j = (j_1, j_2)$ and $l = (l_1, l_2)$ satisfy $-2^{N/2+1} \leq j_i, l_i \leq 2^{N/2+1}$ for $N = 8$. In both (a) and (b), we map j and l into standard matrix indices $1, 2, \dots, (2^{N/d} + 1)^d$ by lexicographical ordering. The matrix in (b) is thus equal to the Kronecker product of the matrix in (a) with itself.

and the reproducing kernel and orthonormal basis functions of \mathcal{H} similarly factorize as

$$\begin{aligned} k(x, x') &= k^{(1)}(\theta_1, \theta'_1) \cdots k^{(1)}(\theta_d, \theta'_d), \\ \phi_j(x) &= \varphi_{j_1}(\theta_1) \cdots \varphi_{j_d}(\theta_d), \end{aligned}$$

where $x = (\theta_1, \dots, \theta_d)$, $x' = (\theta'_1, \dots, \theta'_d)$, and $j = (j_1, \dots, j_d)$.

It is also worthwhile noting that in dimension $d = 1$, the scaling factors $e^{-\tau|j|_p/2} = e^{-\tau|j|^p/2}$ are square roots of the eigenvalues of a fractional diffusion semigroup on $L^2(\mu)$ generated by the square root of the Laplacian, with Fourier function ϕ_j the corresponding eigenfunction. Specifically, we have $e^{-\tau\Delta^{p/2}} \phi_j = e^{-\tau|j|^p} \phi_j$, where Δ is the (positive-definite) Laplace-Beltrami operator associated with the standard metric on the circle, $\Delta f = -f''$.

	$L^2(\mu)$	$L^\infty(\mu)$	$C(X)$	$C^\infty(X)$	\mathcal{H}
Completeness	✓	✓	✓	×	✓
Hilbert space structure	✓	×	×	×	✓
Pointwise evaluation	×	×	✓	✓	✓
*-algebra structure	×	✓	✓	✓	✓
C^∞ regularity	×	×	×	✓	✓

TABLE I. Properties of representative spaces of classical observables on a compact abelian group X . The space \mathcal{H} is an RKHA, which, in addition to being an RKHS it has Banach *-algebra structure.

In dimension $d > 1$, the quantities $e^{-\tau|j|_p/2}$ can correspondingly be interpreted as eigenvalues of a fractional diffusion semigroup on $L^2(\mathbb{T}^d)$, given by composition of d processes acting along the d circles in the standard factorization $\mathbb{T}^d = S^1 \times \dots \times S^1$. See Ref. [32] for further details.

B. Representation of observables

1. Classical observables as multiplication operators

Having established a quantum mechanical representation of classical states, we now consider how to represent classical observables by quantum mechanical observables. First, suppose that we are interested in simulating the evolution of a continuous, real-valued observable $f \in C(X)$ with $X = \mathbb{T}^d$ as in the preceding sections. While f need not be an element of the RKHA \mathcal{H} , the fact that \mathcal{H} is a dense subspace of $C(X)$ means that for any error tolerance $\epsilon > 0$, there exists an observable $g \in \mathcal{H}$ such that

$$\|f - g\|_{C(X)} \equiv \max_{x \in X} |f(x) - g(x)| < \epsilon.$$

By virtue of the above, and for simplicity of exposition, henceforth we will assume that f lies in \mathcal{H} , with a tacit understanding that if it lies in $C(X) \setminus \mathcal{H}$ it is possible to approximate it by an element of \mathcal{H} to arbitrarily high precision in $C(X)$ norm. As a concrete example, suppose that $f \in C(X)$ has a Fourier expansion

$$f = \sum_{j \in \mathbb{Z}^d} \hat{f}_j \phi_j \quad \text{with} \quad \hat{f}_j = \langle \phi_j, f \rangle_{L^2(\mu)}$$

with absolutely summable coefficients; i.e., $\sum_{j \in \mathbb{Z}^d} |\hat{f}_j| < \infty$. Then, by results from Fourier analysis on compact groups [33], the spectrally truncated function $f_L := \sum_{|j| \leq L} \hat{f}_j \phi_j$ converges uniformly to f ; that is, for every $\epsilon > 0$, there exists $L_* \geq 0$ such that for $L > L_*$, $\|f - f_L\|_{C(X)} < \epsilon$. Meanwhile, f_L lies in \mathcal{H} , with $\|f_L\|_{\mathcal{H}}^2 = \sum_{|j| \leq L} e^{\tau|j|_p} |\hat{f}_j|^2$, so we can obtain a uniform approximation of f by f_L at any error tolerance ϵ , as desired. It a standard result from Fourier analysis that f_L is real-valued whenever f is, so f_L lies, in fact, in \mathcal{H}_{sa} .

Assuming then that the classical observable f is an element of \mathcal{H} , its quantum mechanical representation is considerably facilitated by the RKHA structure of that space. Specifically, it follows from the Banach algebra property in (11) that for every $f \in \mathcal{H}$ the multiplication operator $M_f : g \mapsto fg$ is well-defined as a bounded operator in $B(\mathcal{H})$. This leads to the so-called regular representation $\pi : \mathcal{H} \rightarrow B(\mathcal{H})$, which is the algebra homomorphism of \mathcal{H} into $B(\mathcal{H})$, mapping classical observables in \mathcal{H} to the corresponding multiplication operator,

$$\pi(f) = M_f. \quad (13)$$

This mapping is a homomorphism since

$$\pi(fg) = M_{fg} = M_f M_g, \quad \forall f, g \in \mathcal{H},$$

and it is injective (i.e., faithful as a representation) since $\pi(f - f')1_X = f - f' \neq 0$ whenever $f \neq f'$. However, π is not a *-representation; i.e., $\pi(f^*)$ is not necessarily equal to M_f^* . In particular, M_f need not be a self-adjoint operator in $B(\mathcal{H})$ if f is a self-adjoint element in \mathcal{H}_{sa} .

To construct a map from \mathcal{H} into the self-adjoint operators in $B(\mathcal{H})$, we define $T : \mathcal{H} \rightarrow B(\mathcal{H})$ with

$$Tf = (\pi(f) + \pi(f)^*)/2; \quad (14)$$

see again the right-hand column of Fig. 2. By construction, Tf is self-adjoint for all $f \in \mathcal{H}$, and it can also be shown (see Appendix A) that the map $f \mapsto S_f$ is injective on \mathcal{H}_{sa} . That is, T provides a one-to-one mapping between \mathcal{H}_{sa} and quantum mechanical observables on \mathcal{H} , i.e., self-adjoint operators in $B(\mathcal{H})$.

It follows from the product formula in (12) that if $f \in \mathcal{H}$ has the expansion $f = \sum_{j \in \mathbb{Z}^d} \tilde{f}_j \psi_j$, where $\tilde{f}_j = \langle \psi_j, f \rangle_{\mathcal{H}}$, then the corresponding multiplication operator $M_f = \pi(f)$ has the matrix elements

$$(M_f)_{ij} := \langle \psi_i, M_f \psi_j \rangle_{\mathcal{H}} = \langle \psi_i, f \psi_j \rangle_{\mathcal{H}} = c_{j, i-j} \tilde{f}_{i-j}. \quad (15)$$

Correspondingly, the matrix elements of the self-adjoint operator $S_f := Tf$ are given by

$$\begin{aligned} (S_f)_{ij} &:= \langle \psi_i, S_f \psi_j \rangle_{\mathcal{H}} = \frac{(M_f)_{ij} + (M_f^*)_{ji}}{2} \\ &= \frac{c_{j, i-j} \tilde{f}_{i-j} + c_{i, j-i} \tilde{f}_{j-i}^*}{2}. \end{aligned}$$

If, in addition, f lies in \mathcal{H}_{sa} , then we have $\tilde{f}_{j-i}^* = \tilde{f}_{i-j}$ and the formula above reduces to

$$(S_f)_{ij} = \frac{c_{j, i-j} + c_{i, j-i}}{2} \tilde{f}_{i-j}. \quad (16)$$

Here, of particular interest are the multiplication and self-adjoint operators representing the basis elements of \mathcal{H} , i.e., M_{ψ_l} and S_{ψ_l} , respectively, for $l \in \mathbb{Z}^d$. Since $\tilde{f}_{i-j} = \delta_{l, i-j}$ for $f = \psi_l$, it follows from (15) that after a suitable lexicographical ordering of multi-indices (as in Fig. 4), $(M_f)_{ij}$ forms a banded matrix with nonzero

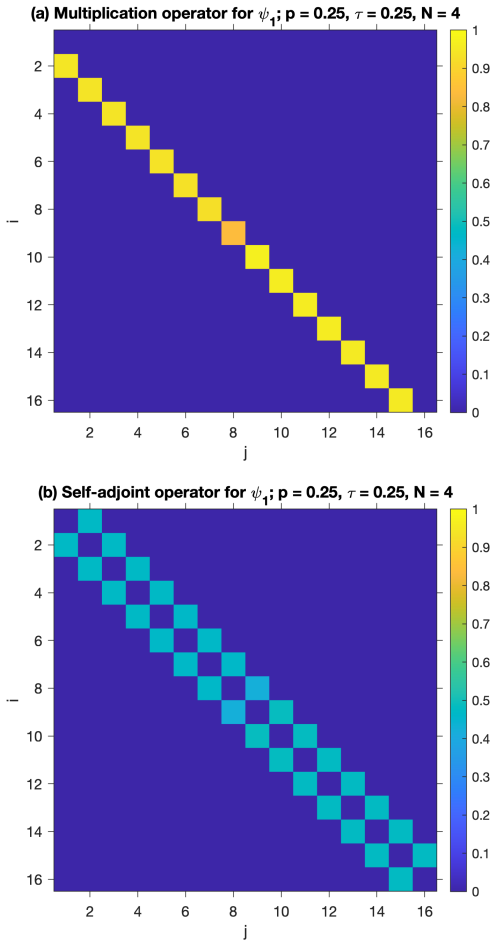


FIG. 5. Matrix elements $(M_{\psi_1})_{ij}$ (a) and $(S_{\psi_1})_{ij}$ (b) of the multiplication and self-adjoint operators representing basis function ψ_1 , respectively, for the RKHA on the circle from Fig. 4(a). The matrix in (a) has nonzero elements only in the first lower diagonal, $i - j = 1$. The matrix in (b) is a symmetric bidiagonal matrix with elements in the first upper and lower diagonals, $i - j = \pm 1$.

elements only in the diagonal corresponding to multi-index k . See Fig. 5 for an illustration. Similarly, S_{ψ_l} is a bi-diagonal matrix with nonzero entries in the diagonals corresponding to ± 1 ; see again Fig. 5.

We deduce from these observations that if f is a bandlimited observable, expressible as a finite linear combination of Fourier functions ϕ_j , M_f is represented by a banded matrix, whose l -th diagonal comprises of the structure constants c_{lj} multiplied by \tilde{f}_l . The matrix representing S_f is also banded whenever f is bandlimited. If, in addition, f is real, the l -th diagonal of $(S_f)_{ij}$ is given by the multiple of $(c_{lj} + c_{li})/2$ with \tilde{f}_l .

2. Classical-quantum consistency

We now come to a key property of the regular representation π and the associated map T , which is a consequence of the reproducing property in (5). Namely, π and T provide a consistent correspondence between evaluation of classical observables and quantum mechanical expectation values. To see this, for any quantum state $\rho \in \mathcal{Q}(\mathcal{H})$ and quantum mechanical observable $A \in B(\mathcal{H})$, let

$$\langle A \rangle_\rho := \text{tr}(\rho A) \quad (17)$$

be the standard quantum mechanical expectation functional. Then, it follows from the reproducing property in (5), the definition of the quantum feature map Q in (7), and the definition of the regular representation in (13) that for any observable $f \in \mathcal{H}$ and classical state $x \in X$,

$$f(x) = \langle \pi(f) \rangle_{\rho_x} = \langle T(f) \rangle_{\rho_x}. \quad (18)$$

The last equation in (18) requires that f is a self-adjoint element in \mathcal{H}_{sa} ; see Ref. [32] for further details. Equation (18) shows, in particular, that by passing to the quantum mechanical representation we maintain consistency with the classical measurement processes for special sets of quantum mechanical observables (the self-adjoint operators T_f in \mathcal{H}) and states (the pure states resulting from the quantum feature map Q).

To express these relationships in terms of matrix elements, note first that the quantum state ρ_x satisfies

$$\begin{aligned} (\rho_x)_{ij} &:= \langle \psi_i, \rho_x \psi_j \rangle_{\mathcal{H}} \\ &= \frac{\langle \psi_i, k_x \rangle_{\mathcal{H}} \langle k_x, \psi_j \rangle_{\mathcal{H}}}{\kappa} \\ &= \frac{\psi_i^*(x) \psi_j(x)}{\kappa}. \end{aligned} \quad (19)$$

Combining this result with (15), we obtain

$$\begin{aligned} f(x) &= \text{tr}(\rho_x \pi(f)) \\ &= \sum_{i,j \in \mathbb{Z}^d} (\rho_x)_{ij} (M_f)_{ji} \\ &= \sum_{i,j \in \mathbb{Z}^d} \frac{\psi_i^*(x) \psi_j(x) c_{i,j-i} \tilde{f}_{j-i}}{\kappa}, \end{aligned}$$

and this relationship holds irrespective of whether f is self-adjoint or not. If f is a self-adjoint element in \mathcal{H}_{sa} , then we can use the matrix elements of the self-adjoint operator S_f from (16), in conjunction with the fact that ρ_x is also self-adjoint, to arrive at the expression

$$\begin{aligned} f(x) &= \text{tr}(\rho_x T(f)) \\ &= \sum_{i,j \in \mathbb{Z}^d} (\rho_x)_{ij} (S_f)_{ji} \\ &= \sum_{i,j \in \mathbb{Z}^d} \frac{\psi_i^*(x) \psi_j(x) (c_{i,j-i} + c_{j,i-j}) \tilde{f}_{j-i}}{2\kappa}. \end{aligned}$$

C. Dynamical evolution

We now turn to the problem of consistently mapping the classical evolution of observables under the torus rotation into a quantum mechanical evolution. From an operator-theoretic perspective, simulating the dynamical evolution of a continuous classical observable $f \in C(X)$ can be understood as approximating the Koopman operator U^t on $C(X)$; for, if U^t were known one could use it to compute $U^t f(x) = f(\Phi^t(x))$ for every observable $f \in C(X)$, time $t \in \mathbb{R}$, and initial condition $x \in X$ (cf. Section II). Yet, despite its theoretical appeal, consistently approximating the Koopman operator on $C(X)$ is challenging in practice, as this space lacks the Hilbert space structure underpinning commonly employed operations employed in numerical techniques, such as orthogonal projections (see Table I). For a measure-preserving, ergodic dynamical system such as the torus rotation in (3), a natural alternative is to consider the unitary Koopman operator on the $L^2(\mu)$ Hilbert space associated with the invariant measure μ . While the choice addresses the absence of orthogonal projections on $C(X)$, $L^2(\mu)$ lacks the notion of pointwise evaluation of functions, so one must correspondingly abandon the notion of pointwise forecasting in this space.

In light of the above considerations, RKHSs emerge as attractive candidates of spaces of classical observables in which to perform simulation, as they allow pointwise evaluation through the reproducing property in (5) while having a Hilbert space structure. Unfortunately, an obstruction to using RKHSs in dynamical systems forecasting is that a general RKHS \mathcal{H} on X need not be preserved under the dynamics, even if the reproducing kernel k is continuous. That is, in general, if f lies in \mathcal{H} , the composition $f \circ \Phi^t$ need not lie in this space, and thus the Koopman operator is not well-defined as an operator mapping \mathcal{H} into itself [34]. Intuitively, this is because membership of a function f in an RKHS generally imposes stringent requirements in its regularity, as we discussed for example in Section III A with the exponential decay of Fourier coefficients, which need not be preserved by the dynamical flow.

An exception to this obstruction occurs when the reproducing kernel k is translation-invariant, which holds true for the class of kernels introduced in Section III A (see Eq. (10)). In fact, it can be shown [35] that for the choice of kernel in (9), the RKHA \mathcal{H} is invariant under the Koopman operator U^t for all $t \in \mathbb{R}$, and $U^t : \mathcal{H} \rightarrow \mathcal{H}$ is unitary and strongly continuous. Analogously to the $L^2(\mu)$ case, the evolution group $\{U^t : \mathcal{H} \rightarrow \mathcal{H}\}_{t \in \mathbb{R}}$ is uniquely characterized through its skew-adjoint generator $V : D(V) \rightarrow \mathcal{H}$, defined on a dense subspace $D(V) \subset \mathcal{H}$, and acting on observables as displayed in Eq. (4).

For the torus rotation in (3), V is diagonalizable in the $\{\psi_j\}$ basis of \mathcal{H} . That is, for $j = (j_1, \dots, j_d)$ we have

$$V\psi_j = i\omega_j\psi_j,$$

where ω_j is a real eigenfrequency given by

$$\omega_j = j_1\alpha_1 + \dots + j_d\alpha_d. \quad (20)$$

Moreover, V admits a decomposition into mutually commuting, skew-adjoint generators V_1, \dots, V_d satisfying

$$V_l\psi_j = ij_l\alpha_l\psi_j. \quad (21)$$

In particular, since $\{\psi_j\}$ is an orthonormal basis, (21) completely characterizes V_l , and we have

$$\begin{aligned} V &= V_1 + \dots + V_d, \\ [V_j, V_l] &= 0, \quad [V_j, V] = 0. \end{aligned} \quad (22)$$

It should be noted that the Koopman group on $L^2(\mu)$ admits a structurally similar decomposition to (22); see e.g., Ref. [36] for further details.

Analogously to the $L^2(\mu)$ case, the generator from (4), the Koopman operator on \mathcal{H} can be recovered at any $t \in \mathbb{R}$ from the generator by exponentiation,

$$U^t = e^{tV}.$$

In addition, there is an induced action $\mathcal{U}^t : B(\mathcal{H}) \rightarrow B(\mathcal{H})$ on quantum mechanical observables in $B(\mathcal{H})$, given by

$$\mathcal{U}^t A = U^t A U^{t*}. \quad (23)$$

This action has the important property of being equivariant with the action of the Koopman operator on functions in \mathcal{H} under the regular representation. Specifically, for every $f \in \mathcal{H}$ and $t \in \mathbb{R}$, we have

$$\mathcal{U}^t \pi(f) = \pi(U^t f).$$

Note that $\{\mathcal{U}^t\}_{t \in \mathbb{R}}$ forms a strongly continuous group of isometries on $B(\mathcal{H})$, whose generator \mathcal{V} acts as a Lie derivative with respect to V on all operators A whose range is included in the domain of V , i.e., $\mathcal{V}A = [V, A]$.

The unitary evolution in (23) has a corresponding dual action $\Psi^t : \mathcal{Q}(\mathcal{H}) \rightarrow \mathcal{Q}(\mathcal{H})$ on quantum states, given by

$$\Psi^t(\rho) = U^{t*} \rho U^t \equiv \mathcal{U}^{-t} \rho. \quad (24)$$

One can verify that for the choice of kernel in (9), this action has the property of being equivariant with the classical dynamical flow, viz.

$$\Psi^t(\rho_x) = \rho_{\Phi^t(x)},$$

where $\rho_x = Q(x) \in \mathcal{Q}(\mathcal{H})$ is the quantum mechanical state representing the classical state $x \in X$ as described in Section III A. Using (18), (23), and (24), we arrive at the consistency relationships

$$\begin{aligned} U^t f(x) &= \langle \mathcal{U}^t M_f \rangle_{\rho_x} = \langle M_f \rangle_{\Psi^t(\rho_x)} \quad \text{and} \\ M_f &= \pi(f), \end{aligned} \quad (25)$$

which hold for every classical observable $f \in \mathcal{H}$, initial condition $x \in X$, and evolution time $t \in \mathbb{R}$. If, in addition, f is a self-adjoint element in \mathcal{H}_{sa} , we may compute the evolution $U^t f$ using the self-adjoint operator $S_f = T(f)$, which is accessible via physical measurements. That is, for $f \in \mathcal{H}_{\text{sa}}$ we have

$$U^t f(x) = \langle U^t S_f \rangle_{\rho_x} = \langle S_f \rangle_{\Psi^t(\rho_x)}. \quad (26)$$

In summary, we have constructed a dynamically consistent embedding of the torus rotation from (3) into a quantum mechanical system on the RKHA \mathcal{H} . For completeness, we note that the matrix elements of the state $\Psi^t(\rho_x)$ are given by

$$\begin{aligned} \langle \psi_i, \Psi^t(\rho_x) \psi_j \rangle_{\mathcal{H}} &= \langle U^t \psi_i, U^t \rho_x \psi_j \rangle_{\mathcal{H}} \\ &= e^{i(\omega_j - \omega_i)t} (\rho_x)_{ij}. \end{aligned}$$

Using this formula together with the expressions for the matrix elements of M_f and S_f in (15) and (16), respectively, we arrive at the expression

$$U^t f = \sum_{i,j \in \mathbb{Z}^d} e^{i(\omega_j - \omega_i)t} \frac{\psi_i^*(x) \psi_j(x) (c_{i,j-i} + c_{j,i-j}) \tilde{f}_{j-i}}{2\kappa},$$

which holds for all self-adjoint $f = \sum_{j \in \mathbb{Z}^d} \tilde{f}_j \psi_j \in \mathcal{H}_{\text{sa}}$.

D. Finite-dimensional approximation of the quantum system

While being dynamically consistent with the underlying classical evolution, the quantum system constructed in Section III C is infinite-dimensional, and thus not directly accessible to simulation by a quantum computer. We now describe the approach for projecting the infinite-dimensional quantum system to a finite-dimensional system, which (i) is amenable to implementation on a quantum computer taking advantage of quantum parallelism; and (ii) converges to the original system as the dimension increases. The approximation proceeds in two steps. First, we define projection operators for the states and operators on the Hilbert space \mathcal{H} to a finite-rank operators on a finite-dimensional subspace $\mathcal{H}_N \subset \mathcal{H}$. Secondly, a unitary map is applied to pass from \mathcal{H}_N to the tensor product Hilbert space $\mathcal{B}_N = \mathcal{B}^{\otimes N}$ associated with N qubits.

1. Finite-rank projection

We begin by fixing a positive integer parameter N (the number of qubits), chosen such that it is a multiple of the dimension d of the original state space X , and defining the index sets

$$\begin{aligned} J^{(1)} &= \{-2^{N/d-1}, \dots, -1, 1, \dots, 2^{N/d-1}\}, \\ J &= \{(j_1, \dots, j_d) \in \mathbb{Z}^d : j_i \in J^{(1)}\}. \end{aligned} \quad (27)$$

Note that the number of elements of J is $L \equiv 2^N$. Next, consider the L -dimensional subspace of \mathcal{H} given by

$$\mathcal{H}_N = \text{span}\{\psi_j : j \in J\},$$

and $\Pi_N : \mathcal{H} \rightarrow \mathcal{H}$ the orthogonal projection mapping into \mathcal{H}_N . Note that \mathcal{H}_N has the structure of an RKHS of dimension 2^N , associated with the spectrally truncated reproducing kernel

$$k_N(x, x') = \sum_{j \in J} \psi_j^*(x) \psi_j(x').$$

We also introduce the infinite index set

$$J_0 = \{(j_1, \dots, j_d) \in \mathbb{Z}^d : j_i \neq 0\},$$

as well as the corresponding infinite-dimensional closed subspace

$$\mathcal{H}_0 = \overline{\text{span}\{\psi_j : j \in J_0\}},$$

and orthogonal projection $\Pi_0 : \mathcal{H} \rightarrow \mathcal{H}$ with $\text{ran } \Pi_0 = \mathcal{H}_0$. The space \mathcal{H}_0 is then an RKHS associated with the kernel

$$k_0(x, x') = \sum_{j \in J_0} \psi_j^*(x) \psi_j(x').$$

Note that $\mathcal{H}_1, \mathcal{H}_2, \dots$ is a nested family of subspaces, increasing towards \mathcal{H}_0 .

By virtue of being spanned by eigenfunctions of the generator V , \mathcal{H}_N is invariant under the Koopman operator, i.e., $U^t \mathcal{H}_N = \mathcal{H}_N$ for all $t \in \mathbb{R}$. Moreover, the projection Π_N commutes with both V and U^t ,

$$[V, \Pi_N] = 0, \quad [U^t, \Pi_N] = 0.$$

These invariance properties allow us to define a projected generator

$$V_N = V \Pi_N \equiv \Pi_N V \Pi_N,$$

and an associated Koopman operator

$$U_N^t := e^{tV_N} \equiv U^t \Pi_N \equiv \Pi_N U^t \Pi_N,$$

such that the following diagram commutes for all $t \in \mathbb{R}$:

$$\begin{array}{ccc} \mathcal{H} & \xrightarrow{U^t} & \mathcal{H} \\ \downarrow \Pi_N & & \downarrow \Pi_N \\ \mathcal{H} & \xrightarrow{U_N^t} & \mathcal{H} \end{array} \quad (28)$$

Similarly, we define a finite-rank Heisenberg operator

$$\mathcal{U}_N^t := \mathcal{U}^t \tilde{\Pi}_N \equiv \tilde{\Pi}_N \mathcal{U}^t \equiv \tilde{\Pi}_N \mathcal{U}^t \tilde{\Pi}_N,$$

where $\tilde{\Pi}_N : B(\mathcal{H}) \rightarrow B(\mathcal{H})$ is the projection on $B(\mathcal{H})$ defined as $\tilde{\Pi}_N A = \Pi_N A \Pi_N$. This leads to an analogous commutative diagram to that in (28) viz.,

$$\begin{array}{ccc} B(\mathcal{H}) & \xrightarrow{\mathcal{U}^t} & B(\mathcal{H}) \\ \downarrow \tilde{\Pi}_N & & \downarrow \tilde{\Pi}_N \\ B(\mathcal{H}) & \xrightarrow{\mathcal{U}_N^t} & B(\mathcal{H}) \end{array}$$

The projected generator $V_0 := \Pi_0 V \Pi_0$, Koopman operator $U_0^t = e^{tV_0}$, and Heisenberg operator $\mathcal{U}_0^t = \tilde{\Pi}_0 \mathcal{U}_t$ with $\tilde{\Pi}_0 A = \Pi_0 A \Pi_0$ satisfy analogous relationships to their finite-rank counterparts, which we do not reproduce here for brevity.

Next, we introduce a spectrally truncated feature map $F_N : X \rightarrow \mathcal{H}$, defined analogously to (6) as

$$F_N(x) = k_{x,N} := k_N(x, \cdot),$$

as well as a corresponding quantum feature map $Q_N : X \rightarrow \mathcal{Q}(\mathcal{H})$ with $Q_N(x) = \rho_{x,N}$,

$$\begin{aligned} \rho_{x,N} &= \langle \xi_{x,N}, \cdot \rangle_{\mathcal{H}} \xi_{x,N} \quad \text{with} \\ \xi_{x,N} &= \frac{k_{x,N}}{\kappa_N}, \quad \kappa_N = k_N(x, x) = \sum_{j \in J} e^{-\tau|j|_p}. \end{aligned} \quad (29)$$

We also set $F_0 : X \rightarrow \mathcal{H}$ and $Q_0 : X \rightarrow \mathcal{Q}(\mathcal{H})$ analogously to F_N and Q_N , respectively, with k_N replaced by k_0 . In the sequel, we will use the states $\rho_{x,N}$ as approximations of the states $\rho_{x,0}$ associated with the quantum feature map from (7). These approximations have the following important properties.

1. The dynamical evolution of $\rho_{x,N}$ can be described, without approximation, using the finite-rank operator \mathcal{U}_N^t ; that is,

$$\Psi^t(\rho_{x,N}) = \mathcal{U}^{-t} \rho_{x,N} = \mathcal{U}_N^{-t} \rho_{x,N}.$$

2. The expectation value of any quantum mechanical observable $A \in B(\mathcal{H})$ with respect to $\rho_{x,N}$ is equal to the expectation value of the finite-rank observable $A_N := \tilde{\Pi}_N A$, i.e.,

$$\langle A \rangle_{\rho_{x,N}} = \langle A_N \rangle_{\rho_{x,N}}.$$

3. As $N \rightarrow \infty$ (i.e., in the infinite qubit limit), $\rho_{x,N}$ converges to $\rho_{x,0}$, in the sense that for any quantum mechanical observable $A \in B(\mathcal{H})$,

$$\langle A \rangle_{\rho_{x,N}} \xrightarrow{N \rightarrow \infty} \langle A \rangle_{\rho_{x,0}}, \quad (30)$$

where the convergence is uniform with respect to $x \in X$.

In addition, the quantum feature map Q_0 allows us to consistently recover all predictions made for classical observables using Q from (7), as we now describe. First, observe that by definition of $\rho_{x,0}$ and ρ_x , if $A \in B(\mathcal{H})$ is a quantum mechanical observable whose range is included in \mathcal{H}_0 and whose nullspace includes the orthogonal complement \mathcal{H}_0^\perp , then

$$\langle A \rangle_{\rho_x} = \frac{\kappa_0}{\kappa} \langle A \rangle_{\rho_{x,0}}. \quad (31)$$

That is, for all observables in this class, expectation values with respect to ρ_x can be recovered from expectation values with respect to $\rho_{x,0}$ up to a constant scaling factor.

For our purposes, this means that the quantum mechanical observables $M_{f,0} = \pi_0(f)$ and $S_{f,0} = T_0(f)$ obtained through the projections $\pi_0 = \tilde{\Pi}_0 \pi$ and $T_0 = \tilde{\Pi}_0 T$ of π and T from (13) and (14), respectively, satisfy (31).

What remains in order to arrive at a consistency relation between classical function evaluation and quantum mechanical expectation, analogous to (18), is to introduce a suitable modification of these maps to account for scaling errors. Such modifications are found to be

$$\tilde{\pi}_0 = \pi_0 \circ \mathcal{L}_0, \quad \tilde{T}_0 = T_0 \circ \mathcal{L}_0.$$

In the above, $\mathcal{L}_0 : \mathcal{H} \rightarrow \mathcal{L}$ is a compact, self-adjoint operator which is diagonal in the $\{\psi_j\}$ basis of \mathcal{L} , and defined through the eigenvalue equation

$$\mathcal{L}_0 \psi_j = \left(1 - \frac{e^{-\tau|j|_p}}{\kappa_0}\right)^{-1} \psi_j.$$

With this definition, one can verify that for every $x \in X$ the following classical–quantum consistency relation holds,

$$f(x) = \langle \tilde{\pi}_0(f) \rangle_{\rho_{x,0}} = \langle \tilde{T}_0(f) \rangle_{\rho_{x,0}}, \quad (32)$$

where in the first equality f is an arbitrary element of \mathcal{H} and in the second equality f is a real-valued observable in \mathcal{H}_{sa} .

In light of the above, we employ the following approximations to the quantum mechanical representation of classical observables from (25) and (26), respectively,

$$\begin{aligned} \tilde{f}_{t,N}(x) &:= \langle M_{f,N} \rangle_{\Psi^t(\rho_{x,N})}, \\ f_{t,N}(x) &:= \langle S_{f,N} \rangle_{\Psi^t(\rho_{x,N})}, \end{aligned} \quad (33)$$

where

$$\begin{aligned} M_{f,N} &= \tilde{\pi}_N f, \quad S_{f,N} = \tilde{T}_N f, \\ \tilde{\pi}_N &= \tilde{\Pi}_N \circ \pi \circ \mathcal{L}_N, \quad \tilde{T}_N = \tilde{\Pi}_N \circ T \circ \mathcal{L}_N. \end{aligned} \quad (34)$$

In (34), \mathcal{L}_N is the self-adjoint, diagonal operator defined analogously to \mathcal{L}_0 by

$$\mathcal{L}_N \psi_j = \left(1 - \frac{e^{-\tau|j|_p}}{\kappa_N}\right)^{-1} \psi_j.$$

By (30), for every function $f \in \mathcal{H}$ and evolution time $t \in \mathbb{R}$, $\tilde{f}_{t,N}(x)$ converges as $N \rightarrow \infty$ to $U^t f(x)$, uniformly with respect to $x \in X$, whereas $f_{t,N}(x)$ converges to $U^t f(x)$ if f is self-adjoint (real-valued). It is important to note that the approximations in (33) are intrinsically quantum mechanical in nature; that is, they are not induced by a classical statistical approximation. More specifically, unlike the feature map Q in (7), Q_N is not expressible as a composition $P \circ \delta$ involving an embedding (δ) of the classical space into the space of classical probability measures, followed by an embedding of the latter (P) into the quantum mechanical state space. In particular, there may be no classical probability measure in $\mathcal{P}(X)$ giving the approximations in (33) as expectation values.

2. Tensor product factorization

Being expressible in terms of finite-rank quantum states, observables, and evolution operators, the approximation framework described in Section III D 1 can be encoded in a quantum computing system operating on a finite-dimensional Hilbert space. In particular, letting $\mathcal{B} \simeq \mathbb{C}^2$ denote the 2-dimensional Hilbert space associated with a single qubit, it follows immediately from the fact that \mathcal{H}_N is a 2^N -dimensional Hilbert space that there exists a unitary map $W_N : \mathcal{H}_N \rightarrow \mathcal{B}_N$, where

$$\mathcal{B}_N := \mathcal{B}^{\otimes N} \simeq \underbrace{\mathbb{C}^2 \otimes \dots \otimes \mathbb{C}^2}_N \quad (35)$$

is the tensor product Hilbert space associated with N qubits. Under such a unitary, the finite-rank generator V_N maps to a skew-adjoint operator $\hat{V} := W_N V_N W_N^*$, inducing a self-adjoint Hamiltonian

$$\hat{H} := \hat{V}/i \quad (36)$$

and a corresponding unitary evolution operator $\hat{U}^t := e^{i\hat{H}t}$ on \mathcal{B}_N . This leads to the commutative diagram

$$\begin{array}{ccc} \mathcal{H}_N & \xrightarrow{U_N^t} & \mathcal{H}_N \\ \downarrow W_N & & \downarrow W_N \\ \mathcal{B}_N & \xrightarrow{\hat{U}^t} & \mathcal{B}_N \end{array}$$

expressing the fact that functions in \mathcal{H}_N and \mathcal{B}_N evolve consistently under U_N^t and \hat{U}^t , respectively. Note that we work here with the self-adjoint Hamiltonian \hat{H} as opposed to the skew-adjoint generator \hat{V} for consistency with the usual convention in quantum mechanics.

In addition, W_N induces a unitary $\mathcal{W}_N : B(\mathcal{H}_N) \rightarrow B(\mathcal{B}_N)$, with $\mathcal{W}_N A = W_N A W_N^*$, mapping quantum mechanical observables on \mathcal{H}_N to quantum mechanical observables on \mathcal{B}_N . The restriction of \mathcal{W}_N on $\mathcal{Q}(\mathcal{H}_N) \subset B(\mathcal{H}_N)$ then induces a continuous, invertible map $\mathcal{W}_N : \mathcal{Q}(\mathcal{H}_N) \rightarrow \mathcal{Q}(\mathcal{B}_N)$ from quantum states on \mathcal{H}_N to quantum states on \mathcal{B}_N (which we continue to denote using the symbol \mathcal{W}_N). Moreover, we have the unitary evolution $\hat{U}^t : B(\mathcal{B}_N) \rightarrow B(\mathcal{B}_N)$ with $\hat{U}^t A = \hat{U}^t A \hat{U}^{t*}$ and the evolution $\hat{\Psi}^t : \mathcal{Q}(\mathcal{B}_N) \rightarrow \mathcal{Q}(\mathcal{B}_N)$ such that the following two diagrams commute:

$$\begin{array}{ccc} B(\mathcal{H}_N) & \xrightarrow{U_N^t} & B(\mathcal{H}_N) & \quad & \mathcal{Q}(\mathcal{H}_N) & \xrightarrow{\Psi^t} & \mathcal{Q}(\mathcal{H}_N) \\ \downarrow \mathcal{W}_N & & \downarrow \mathcal{W}_N & , & \downarrow \mathcal{W}_N & & \downarrow \mathcal{W}_N \\ B(\mathcal{B}_N) & \xrightarrow{\hat{U}^t} & B(\mathcal{B}_N) & & \mathcal{Q}(\mathcal{B}_N) & \xrightarrow{\hat{\Psi}^t} & \mathcal{Q}(\mathcal{B}_N) \end{array}$$

Forming the composition $\hat{\mathcal{W}}' = \mathcal{W}_N \circ \mathcal{S}_N \circ \tilde{\Pi}_N$, where $\mathcal{S}_N : B(\mathcal{H}) \rightarrow B(\mathcal{H})$ is the scaling operator by κ/κ_N , then leads to the following correspondence between the infinite-dimensional quantum system on \mathcal{H} and the finite-

dimensional quantum system associated with the quantum computer,

$$\begin{array}{ccc} \mathcal{Q}(\mathcal{H}) & \xrightarrow{\Psi^t} & \mathcal{Q}(\mathcal{H}) \\ \downarrow \hat{\mathcal{W}}' & & \downarrow \hat{\mathcal{W}}' \\ \mathcal{Q}(\mathcal{B}_N) & \xrightarrow{\hat{\Psi}^t} & \mathcal{Q}(\mathcal{B}_N) \end{array} ,$$

which constitutes the bottom commutative loop in the left-hand column of Fig. 2.

In order for the representation of the dynamics on \mathcal{B}_N to exhibit robust quantum parallelism, i.e., implementation on a quantum circuit of small depth, it is highly beneficial that the Hamiltonian \hat{H} can be decomposed as a sum of commuting operators in pure tensor product form, i.e.,

$$\hat{H} = \sum_{j \in J} \hat{H}_j, \quad (37)$$

where $[\hat{H}_j, \hat{H}_l] = 0$, $\hat{H}_j = \hat{H}_{1j} \otimes \hat{H}_{2j} \otimes \dots \otimes \hat{H}_{Nj}$, and $\hat{H}_{nj} : \mathcal{B} \rightarrow \mathcal{B}$ are mutually-commuting, single-qubit Hamiltonians. It then follows that the unitary operator $\hat{U}^t = e^{i\hat{H}t}$ generated by \hat{H} factorizes as

$$\hat{U}^t = e^{i\sum_{j \in J} \hat{H}_j t} = \prod_{j \in J} e^{i\hat{H}_j t} = \prod_{j \in J} e^{\otimes_{n=1}^N i\hat{H}_{nj} t}, \quad (38)$$

Thus, \hat{U}^t can be split into a composition of up to 2^N unitaries $e^{i\hat{H}_j t}$ (depending on the number of nonzero terms \hat{H}_j in the right-hand side of (37)), which can be applied in any order by commutativity of the \hat{H}_j . Moreover, each unitary $e^{i\hat{H}_j t}$ has a generator of pure tensor product form, and thus can be represented as a quantum circuit with at most N quantum gates for rotations of the individual qubits.

In fact, as we will now show, by virtue of the decomposition of the generator in (22), for a quasiperiodic dynamical system on \mathbb{T}^d , the decomposition in (37) only has N nonzero terms \hat{H}_j , and for each nonzero term, the tensor product factorization $\hat{H}_j = \otimes_{n=1}^N \hat{H}_{nj}$ has all but one factors \hat{H}_{nj} equal to the identity. As a result,

$$e^{\otimes_{n=1}^N i\hat{H}_{nj} t} = \bigotimes_{n=1}^N e^{i\hat{H}_{nj} t},$$

and the decomposition in (38) reduces to a tensor product of N unitaries,

$$\hat{U}^t = \bigotimes_{n=1}^N \hat{U}_n^t, \quad \hat{U}_n^t = e^{i\sum_{j \in J} \hat{H}_{nj} t}. \quad (39)$$

The key point about (39) is that \hat{U}^t can be implemented via a quantum circuit of N qubit channels with no cross-channel communication (and thus also no additional entanglement), significantly enhancing error tolerance.

3. Walsh operator representation

Classical states and observables of the dynamical system have been transformed into pure state density operators and self-adjoint operators in the 2^N -dimensional Hilbert space \mathcal{B}_N which is a tensor product of the single qubit quantum state spaces as given in (35). For the rest of this section we switch to the commonly used Dirac bra-ket notation [5]. We let $\{|0\rangle, |1\rangle\}$ be the standard orthonormal basis of the single-qubit Hilbert space $\mathcal{B} \simeq \mathbb{C}^2$ comprising of eigenvectors of the Pauli Z operator,

$$Z|0\rangle = |0\rangle, \quad Z|1\rangle = -|1\rangle.$$

Thus, each vector $|\psi\rangle \in \mathcal{B}$ can be expanded in this basis as

$$|\psi\rangle = \alpha|0\rangle + \beta|1\rangle \quad \text{with} \quad \alpha, \beta \in \mathbb{C}. \quad (40)$$

In order to arrive at the decomposition in (39), we employ the approach developed in Ref. [37], which is based on discrete Walsh-Fourier transforms, and the associated Walsh operators, as follows. First, for any non-negative integer $n \in \mathbb{N}_0$, we let $\beta(n) = (\beta_1(n), \dots, \beta_N(n)) \in \{0, 1\}^N$ be its binary expansion. That is,

$$n = \sum_{i=1}^N \beta_i(n) 2^{i-1},$$

where N is the smallest integer such that $n \leq 2^N - 1$. Moreover, for every real number $u \in [0, 1)$ we let $\gamma(u) = (\gamma_1(u), \gamma_2(u), \dots) \in \{0, 1\}^{\mathbb{N}}$ be its dyadic expansion, i.e.,

$$\gamma(u) = \sum_{i=1}^{\infty} \frac{\gamma_i(u)}{2^i}.$$

Note that the most significant digit in $\beta(n)$ is the last one, $\beta_N(n)$, whereas the most significant digit in $\gamma(u)$ is the first one, $\gamma_1(u)$. Using $\tilde{\beta}(n) = (\beta_N(n), \beta_{N-1}(n), \dots, \beta_1(n))$ to denote the bit-reversed binary representation of n , we have $\gamma_i(n/2^N) = \tilde{\beta}_i(n)$.

With this notation, for every $n \in \mathbb{N}_0$ we define the *Walsh function* $w_n : [0, 1) \rightarrow \{0, 1\}$, where

$$w_n(u) = (-1)^{\sum_{i=1}^N \beta_i(n) \gamma_i(u)}.$$

Furthermore, for any $N \in \mathbb{N}$ and $n \in \{0, \dots, 2^N - 1\}$, we define the discrete Walsh function of order N , $w_n^{(N)} : \{0, \dots, 2^N - 1\} \rightarrow \{0, 1\}$, as

$$w_n^{(N)}(m) = w_n(m/2^N) \quad \text{with} \quad m = 0, \dots, 2^N - 1.$$

Note that

$$\begin{aligned} w_n(m/2^N) &= (-1)^{\sum_{i=1}^N \beta_i(n) \gamma_i(m/2^N)} \\ &= (-1)^{\sum_{i=1}^N \beta_i(n) \tilde{\beta}_i(m)}, \end{aligned}$$

so the exponent in the expression for $w_n^{(N)}(m)$ is given by the inner product between the binary expansion of

n with the *bit-reversed* binary expansion of m . Among the Walsh functions w_n , those with $n = 1, 2, 4, \dots, 2^l$ for $l \in \mathbb{N}_0$ are called *Rademacher functions*, R_l , and satisfy

$$w_{2^l}(u) \equiv R_l(u) = (-1)^{\gamma_l(u)}. \quad (41)$$

That is, $R_l(u)$ depends only on the $(l+1)$ -th bit in the dyadic expansion of u . Using (41), it follows that for any integer $m \in \{0, \dots, 2^N - 1\}$, we have

$$\frac{m}{2^N} = \sum_{i=0}^{N-1} \frac{1 - R_{i+1}(m/2^N)}{2^{i+2}},$$

meaning that we can express the i -th bit in the dyadic decomposition of $m/2^N$ in terms of the $(i-1)$ -th Rademacher function,

$$\gamma_i(m/2^N) = \frac{1 - R_{i-1}(m/2^N)}{2}. \quad (42)$$

It is known that the set $\{w_n\}_{n \in \mathbb{N}_0}$ forms an orthonormal basis of the Hilbert space $L^2([0, 1])$ with respect to Lebesgue measure. In the discrete case, we let $L_N^2([0, 1])$ be the 2^N -dimensional Hilbert space with respect to the normalized counting measure supported on $\{0, 1/2^N, \dots, 1 - 2^{-N}\}$. Then, the set of discrete Walsh functions of order N , $\{w_n^{(N)}\}$, is an orthonormal basis of the Hilbert space $L_N^2([0, 1])$. One obtains

$$\begin{aligned} f &= \sum_{n=0}^{2^N-1} \hat{f}_n w_n^{(N)} \quad \text{with} \\ \hat{f}_n &= \frac{1}{2^N} \sum_{m=0}^{2^N-1} \hat{w}_n(m) f(m/2^N). \end{aligned}$$

The map $\mathcal{F}_N : L_N^2([0, 1]) \rightarrow \mathbb{C}^{2^N}$ with $\mathcal{F}_N f = (\hat{f}_0, \dots, \hat{f}_{2^N-1})$ is called the *discrete Walsh-Fourier transform* of the function $f \in L_N^2([0, 1])$.

Next, consider the tensor product basis $\{|e_b\rangle = |e_{b_1}\rangle \otimes \dots \otimes |e_{b_N}\rangle\}$ of \mathcal{B}_N with $|e_{b_i}\rangle \in \{|0\rangle, |1\rangle\}$, where the multi-index $b = (b_1, \dots, b_N) \in \{0, 1\}^N$ runs over all binary strings of length N . For every $b \in \{0, 1\}^N$, we define the associated *Walsh operator* $Z_b : \mathcal{B}_N \rightarrow \mathcal{B}_N$ as

$$Z_b = Z^{b_1} \otimes Z^{b_2} \otimes \dots \otimes Z^{b_N}.$$

By construction, the Z_b form a collection of mutually-commuting, self-adjoint operators, which have pure tensor product form and are diagonal in the basis $\{|e_b\rangle\}$ of \mathcal{B}_N , i.e.,

$$Z_b |e_c\rangle = \left(\prod_{i=1}^N (-1)^{b_i(c_i-1)} \right) |e_c\rangle.$$

For example, for the 2-qubit case $N = 2$ and the basis vector $|e_c\rangle = |0\rangle \otimes |1\rangle$, one obtains

$$Z_b |e_c\rangle = (I \otimes Z) |e_c\rangle = -|e_c\rangle.$$

In particular, it follows from a counting argument that the collection $\{Z_b\}$ forms a basis of the vector space of operators in $B(\mathcal{B}_N)$ which are diagonal in the $\{|e_b\rangle\}$ basis.

In Ref. [37], it was shown that if $A \in \mathcal{B}(B_N)$ is such a diagonal operator,

$$A|e_c\rangle = a_c|e_c\rangle \quad \text{with} \quad |e_c\rangle \in \{|0\rangle, |1\rangle\}^{\otimes N}, \quad a_c \in \mathbb{C},$$

then it admits the expansion

$$A = \sum_{n=0}^{2^N-1} \hat{f}_n Z_{\beta(n)}, \quad \hat{f}_n \in \mathbb{C}, \quad (43)$$

where the expansion coefficients \hat{f}_n are the complex Walsh-Fourier coefficients $(\hat{f}_0, \dots, \hat{f}_{2^N-1}) = \mathcal{F}_N f$ of the function $(f_0, \dots, f_{2^N-1} \in L_N^2([0, 1])$ with $f_m = a_{\beta(m)}$. That is, f_m is equal to the eigenvalue a_c , where c is the binary representation of integer n .

Next, in order to effect the decomposition in (37) for the generator-induced Hamiltonian from (36), let $\zeta : J^{(1)} \rightarrow \{0, \dots, 2^{N/d} - 1\}$ be the standard order on the index set $J^{(1)}$ from (27) with $\zeta(-2^{N/d-1}) = 0, \dots, \zeta(2^{N/d-1}) = 2^{N/d} - 1$. We define $W_N : \mathcal{H}_N \rightarrow \mathcal{B}_N$ as the unique (unitary) linear map such that for $j = (j_1, \dots, j_d)$,

$$W_N|\psi_j\rangle = |e_c\rangle \quad \text{with} \\ c = \bar{\eta}(j) := (\eta(j_1), \dots, \eta(j_d)), \quad \eta(j_i) = \tilde{\beta}(\zeta(j_i)).$$

That is, W_N maps the basis element $|\psi_j\rangle$ of \mathcal{H}_N with $j \in J$ to the tensor product basis element $|e_c\rangle$, with c given by an invertible binary string encoding of the multi-index $j = (j_1, \dots, j_d)$. Here, c is obtained as a concatenation $(\eta(j_1), \dots, \eta(j_d))$ of d binary strings of length N/d , corresponding to the dyadic decompositions of $\zeta(j_1), \dots, \zeta(j_d)$, respectively.

Since $V|\psi_j\rangle = i\omega_j|\psi_j\rangle$ with ω_j given by (20), we have

$$H|e_c\rangle = \omega_{\bar{\eta}^{-1}(c)}|e_c\rangle, \quad (44)$$

so in order to decompose H into Walsh operators as in (43), we need to compute the discrete Walsh transform of the function $h \in L_N^2([0, 1])$ with

$$h(m/2^N) = \omega_{\eta^{-1}(\tilde{\beta}(m))}.$$

This calculation is detailed in Appendix B. By virtue of the resulting decomposition in (B1), the only nonzero coefficients in the Walsh-Fourier transform $\hat{h} = (\hat{h}_0, \dots, \hat{h}_{2^N-1}) = \mathcal{F}_N h$ are the coefficients \hat{h}_n with $n = 2^{l+(i-1)d}$ and $1 \leq l \leq N/d, 1 \leq i \leq d$. Correspondingly, the only nonzero terms $\hat{a}_b Z_b$ in the Walsh operator expansion from (43) for the Hamiltonian in (44) are those for which the binary string b in Z_b has exactly one bit equal to 1 and the remaining $N - 1$ bits equal to 0. In

particular, we have

$$\begin{aligned} \hat{H} &= \sum_{i=1}^d \sum_{l=0}^{\frac{N}{d}-1} \hat{h}_{2^{l+(i-1)N/d}} Z_{\beta(2^{l+(i-1)N/d})} \\ &= \hat{h}_1 Z \otimes I \otimes I \otimes I \otimes \dots \otimes I \\ &\quad + \hat{h}_2 I \otimes Z \otimes I \otimes I \otimes \dots \otimes I \\ &\quad + \hat{h}_4 I \otimes I \otimes Z \otimes I \otimes \dots \otimes I + \dots \\ &\quad + \hat{h}_{2^{N-1}} I \otimes \dots \otimes I \otimes Z, \end{aligned} \quad (45)$$

which verifies the assertion made in Section III D 2 that the decomposition of \hat{H} in (37) can be arranged to have N nonzero terms, each of which factorizes as a tensor product of N operators, with all but one factors equal to the identity. Since

$$e^{itI \otimes \dots \otimes I \otimes Z \otimes I \otimes \dots \otimes I} = I \otimes \dots \otimes I \otimes e^{itZ} \otimes I \otimes \dots \otimes I,$$

we conclude that

$$\hat{U}^t = e^{i\hat{H}t} = e^{it\hat{h}_1 Z} \otimes e^{it\hat{h}_2 Z} \otimes e^{it\hat{h}_4 Z} \otimes \dots \otimes e^{it\hat{h}_{2^{N-1}} Z},$$

which is consistent with the decomposition in (39).

E. Measurement process

1. Projective measurement

We now describe how to realize probabilistic predictions of the classical evolution $U^t f$ through a projective measurement of the quantum mechanical observables $S_{f,N}$ from (34) on the quantum states $\Psi_N^t(\rho_{x,N})$, where $\rho_{x,N}$ is given by (29). Let $\hat{S} = \mathcal{W}_N S_{f,N}$ and $\hat{\rho} = \mathcal{W}_N \rho_{x,N}$ be the operators on the tensor product space \mathcal{B}_N representing $S_{f,N}$ and $\rho_{x,N}$, respectively. Let also $\hat{\rho}_t = \Psi^t(\rho_{x,N})$. Since $S_{f,N}$ is unitarily equivalent to \hat{S} and $\Psi^t(\rho_{x,N})$ is unitarily equivalent to $\hat{\rho}_t$, it is sufficient to consider the measurement process for \hat{S} on the state $\hat{\rho}_t$.

To that end, note first that since \hat{S} is a finite-rank, self-adjoint operator, it has a spectral resolution

$$\hat{S} = \sum_{s \in \sigma(\hat{S})} s \hat{P}_s = \sum_{s \in \sigma(\hat{S})} s |s\rangle \langle s|,$$

where $\sigma(\hat{S})$ denotes the spectrum of \hat{S} (i.e., the set of eigenvalues), and $\hat{P}_s \in B(\mathcal{B}_N)$ are the orthogonal projections onto the corresponding eigenspaces. The collection $\{\hat{P}_s\}$ defines a projection-valued measure (PVM) on $\sigma(\hat{S})$, i.e., a map $\mathcal{S} : \Sigma(\sigma(\hat{S})) \rightarrow B(\mathcal{B}_N)$ given by

$$\mathcal{S}(\Omega) = \sum_{s \in \Omega} \hat{P}_s,$$

where $\Sigma(\sigma(\hat{S}))$ is the σ -algebra consisting of all subsets of $\sigma(\hat{S})$. A *projective measurement* of \hat{S} on the quantum

state $\hat{\rho}_t$ then corresponds to a random draw \hat{s} from the set $\sigma(\hat{S})$ with probability

$$\mathbb{P}_{\hat{\rho}_t}(s) = \text{tr}(\hat{\rho}_t P_s).$$

The random draws \hat{s} then have expectation

$$\text{tr}(\hat{\rho}_t \hat{P}_s) = \text{tr}(\Psi^t(\rho_{x,N}) S_{f,N}) = f_{t,N}(x),$$

which is consistent with (33).

Operationally, we can perform a Monte Carlo (ensemble) estimate of $f_{t,N}(x)$ by performing a sequence $\hat{s}_1, \dots, \hat{s}_K$ of measurements of \hat{S} on K independently and identically prepared quantum systems. The ensemble mean,

$$\bar{s}_K := \frac{1}{K} \sum_{k=1}^K \hat{s}_k \quad (46)$$

then converges as $K \rightarrow \infty$ to the expectation $f_{t,N}(x)$. The latter, converges in turn to the true value $U^t f(x)$ in the infinite-qubit limit, $N \rightarrow \infty$; that is, we have

$$\lim_{N \rightarrow \infty} \lim_{K \rightarrow \infty} \bar{s}_K = U^t f(x).$$

2. Implementation using a quantum register

The projective measurement process described in Section III E 1 can be equivalently formulated in terms of a PVM associated with the register of a quantum computing platform. The PVM in question, $\mathcal{E} : \Sigma(\{0,1\}^N) \rightarrow B(\mathcal{B}_N)$, has as its domain the σ -algebra $\Sigma(\{0,1\}^N)$ consisting of all subsets of $\{0,1\}^N$, and is defined as

$$\mathcal{E}(\Omega) = \sum_{b \in \Xi} E_b, \quad \text{with } E_b := |e_b\rangle\langle e_b|.$$

In particular, evaluated on a singleton set $\{b\}$, $E(\{b\}) = E_b$ is equal to the rank-1 orthogonal projection along the standard basis vector $|e_b\rangle$ of \mathcal{B}_N . A measurement of \mathcal{E} on the state $\hat{\rho}_t$ then returns a random string $\beta \in \{0,1\}^N$ with probability

$$\mathbb{P}_{\hat{\rho}_t}(b) = \text{tr}(\hat{\rho}_t E_b). \quad (47)$$

A number of quantum computing platforms and/or standard development kits provide functionality to measure the PVM \mathcal{E} associated with the quantum register.

To take advantage of this functionality for the purpose of measuring the target observable \hat{S} , we begin by considering the eigendecomposition

$$\hat{S}|u_n\rangle = s_n|u_n\rangle,$$

where the eigenvalues s_n are taken from $\sigma(\hat{S})$ with multiplicities as needed, and the eigenvectors $|u_0\rangle, \dots, |u_{2^N-1}\rangle$ form an orthonormal basis of \mathcal{B}_N . We then define the unitary map $\Xi : \mathcal{B}_N \rightarrow \mathcal{B}_N$ such that

$$\Xi|e_{\beta(n)}\rangle = |u_n\rangle.$$

This map diagonalizes \hat{S} , meaning that $\hat{D} := \Xi^* \hat{S} \Xi$ is a diagonal operator which satisfies the eigenvalue problem

$$\hat{D}|e_{\beta(n)}\rangle = s_n|e_{\beta(n)}\rangle.$$

Correspondingly, the PVM \mathcal{E} provides a spectral resolution of \hat{S} ,

$$\hat{S} = \sum_{b \in \{0,1\}^N} s_{\beta^{-1}(b)} E_b,$$

and in addition we have

$$\begin{aligned} \text{tr}(\hat{\rho}_t \hat{S}) &= \text{tr}(\tilde{\rho}_t \hat{D}), \\ \text{tr}(\hat{\rho}_t P_s) &= \sum_{n: s_n = s} \text{tr}(\tilde{\rho}_t E_{\beta(n)}), \end{aligned}$$

where $\tilde{\rho}_t = \Xi \hat{\rho}_t \Xi^*$.

Based on the above, an equivalent sampling strategy to that described in Section III E 1 is to perform K independent measurements $\hat{b}_1, \dots, \hat{b}_K$ of \mathcal{E} , where each $\hat{b}_j \in \{0,1\}^N$ is a random string of N -bits occurring with probability

$$\mathbb{P}_{\hat{\rho}_t}(\hat{b}_j) = \text{tr}(\hat{\rho}_t E_{\hat{b}_j}).$$

Computing

$$\bar{s}_K = \frac{1}{K} \sum_{k=1}^K s_{\hat{b}_k}$$

then leads to an estimator of $f_{t,N}(x)$ that converges as $K \rightarrow \infty$ analogously to the estimator in (46).

IV. NUMERICAL EXAMPLES

A. Quantum circuit implementation

We illustrate the Walsh operator representation developed in Section III D 1 by means of an example case for the two-dimensional torus ($d = 2$; see Fig. 3). We seek to approximate the dynamics using $N = 2 \times 2$ qubits, i.e., using the Hilbert space $\mathcal{B}_4 = \mathcal{B}_2 \otimes \mathcal{B}_2$. The corresponding sequences of binary strings and eigenfrequencies ω_j are listed in Table II for completeness. In each torus dimension we thus get a 2-qubit expansion,

$$h^{(1)} = \sum_{n=0}^3 \tilde{h}_n w_n^{(N=2)} = \tilde{h}_1 w_1^{(N=2)} + \tilde{h}_2 w_2^{(N=2)}$$

which corresponds to either $\eta(j_1) = (0,1), (1,0)$ and $\eta(j_2) = (0,0)$ or $\eta(j_2) = (0,1), (1,0)$ and $\eta(j_1) = (0,0)$ as listed in Table II. These results are combined into the following expansion for the spectral function h of the Hamiltonian H on \mathcal{B}_4 :

$$\begin{aligned} h &= \sum_{n=0}^{2^4-1} \hat{h}_n w_n^{(4)} \\ &= \hat{h}_1 w_1^{(4)} + \hat{h}_2 w_2^{(4)} + \hat{h}_4 w_4^{(4)} + \hat{h}_8 w_8^{(4)}. \end{aligned} \quad (48)$$

(j_1, j_2)	$(\eta(j_1), \eta(j_2))$	m	ω_j
$(-2, -2)$	$((0, 0), (0, 0))$	0	$-2\alpha_1 - 2\alpha_2$
$(-1, -2)$	$((0, 1), (0, 0))$	1	$-1\alpha_1 - 2\alpha_2$
$(+1, -2)$	$((1, 0), (0, 0))$	2	$+1\alpha_1 - 2\alpha_2$
$(+2, -2)$	$((1, 1), (0, 0))$	3	$+2\alpha_1 - 2\alpha_2$
$(-2, -1)$	$((0, 0), (0, 1))$	4	$-2\alpha_1 - 1\alpha_2$
$(-1, -1)$	$((0, 1), (0, 1))$	5	$-1\alpha_1 - 1\alpha_2$
$(+1, -1)$	$((1, 0), (0, 1))$	6	$+1\alpha_1 - 1\alpha_2$
$(+2, -1)$	$((1, 1), (0, 1))$	7	$+2\alpha_1 - 1\alpha_2$
$(-2, +1)$	$((0, 0), (1, 0))$	8	$-2\alpha_1 + 1\alpha_2$
$(-1, +1)$	$((0, 1), (1, 0))$	9	$-1\alpha_1 + 1\alpha_2$
$(+1, +1)$	$((1, 0), (1, 0))$	10	$+1\alpha_1 + 1\alpha_2$
$(+2, +1)$	$((1, 1), (1, 0))$	11	$+2\alpha_1 + 1\alpha_2$
$(-2, +2)$	$((0, 0), (1, 1))$	12	$-2\alpha_1 + 2\alpha_2$
$(-1, +2)$	$((0, 1), (1, 1))$	13	$-1\alpha_1 + 2\alpha_2$
$(+1, +2)$	$((1, 0), (1, 1))$	14	$+1\alpha_1 + 2\alpha_2$
$(+2, +2)$	$((1, 1), (1, 1))$	15	$+2\alpha_1 + 2\alpha_2$

TABLE II. Binary encodings $\bar{\eta}(j) = (\eta(j_1), \eta(j_2))$ and enumeration $m = \hat{\beta}^{-1}(\bar{\eta}(j))$ of the eigenfrequencies ω_j with $j = (j_1, j_2)$ of a quasiperiodic system. Our example case has $d = 2$ dimensions and $N = 4$ qubits are used for the approximation on the quantum computer.

b	Z_b	n	\hat{h}_n
$(1, 0, 0, 0)$	$Z \otimes I \otimes I \otimes I$	1	$-3/2$
$(0, 1, 0, 0)$	$I \otimes Z \otimes I \otimes I$	2	$-1/2$
$(0, 0, 1, 0)$	$I \otimes I \otimes Z \otimes I$	4	$-3/2$
$(0, 0, 0, 1)$	$I \otimes I \otimes I \otimes Z$	8	$-1/2$

TABLE III. Walsh operators Z_b , enumeration $n = \beta(b)$, and expansion coefficient \hat{h}_n in the decomposition of the Hamiltonian H in (45) for the quasiperiodic system in Table II with $d = 2$ and an approximation by $N = 4$ qubits. See Fig. 6 for a Qiskit implementation.

The values of the nonzero coefficients \hat{h}_n that result from Table II are displayed in Table III. Thus, the unitary evolution operator is given by

$$\hat{U}^t = e^{-it\frac{3\omega_1}{2}Z} \otimes e^{-it\frac{\omega_2}{2}Z} \otimes e^{-it\frac{\omega_4}{2}Z} \otimes \dots \otimes e^{-it\frac{3\omega_8}{2}Z}, \quad (49)$$

in this example.

Figure 6 displays the quantum circuit that advances the unitary evolution by one time step $t = 0.1$. The implementation is done with Qiskit [24]. As can be seen, there is no communication between the four qubit channels generated in this example. The global phase gates which are applied to qubits $q1_0, q1_1, q1_2$, and $q1_3$ are applied here to perform the exact transformation.

B. Simulated quantum computation

In this section, we illustrate the behavior of the finite-dimensional quantum system produced by the compiler with simulated prediction experiments for observable $f(x) = \sin x$ of a circle rotation (i.e., dimension $d = 1$) of frequency $\alpha = 1$. We have implemented the quantum state and operator matrices described in Section III in

Matlab, using the decomposition

$$f(x) = \sin(x) = e^{\tau/2} \frac{\psi_1(x) + \psi_{-1}(x)}{2i}$$

of our target observable in the RKHA basis. Our objective is to assess the consistency of probabilistic predictions for the evolution $f_t(x) := f(\Phi^t(x)) = \sin(x + \alpha t)$ obtained by the PVM of the self-adjoint observable $S_{f,N}$ from (34), evaluated on the time-dependent quantum state $\Psi^t(\rho_{x,N})$ of the quantum computer, as the number N of qubit increases. We work throughout with the RKHA parameters $p = \tau = 1/4$.

We begin in Fig. 7 with plots of the eigenvalues s_j and representative corresponding eigenfunctions u_j of $S_{f,N}$ for values of N in the range 3–7. There, it is evident that as N increases, the spectrum of $S_{f,N}$ samples the interval $[-1, 1]$, i.e., the range of values of f , with increasingly high density, exhibiting a clustering of eigenvalues near $\{-1, 1\}$. The latter is consistent with the distribution on the range of f induced by a fixed-frequency rotation on the circle. Meanwhile, as N increases, the eigenfunctions exhibit increasingly high localization, with eigenfunction $u_j(x)$ concentrated on points $x \in \mathbb{T}^1$ such that $f(x)$ is close to the corresponding eigenvalue s_j . Thus, intuitively, as N increases the PVM associated with $S_{f,N}$ provides increasingly high resolution in the representation of the classical observable f .

Next, in Fig. 8 we compare the evolution $f_t(x)$ of the true signal for initial state $x = 0$ against the quantum mechanical expectation $f_{t,N}(x)$ from (33) and the probability density on $[-1, 1]$ induced by the PVM for $S_{f,N}$. The latter is equivalent to the probability density induced by the PVM for \hat{S} , as described in Section III E. Note that we assign a probability density to each eigenvalue s_j in the spectrum of $S_{f,N}$ by dividing the probability $\mathbb{P}_{\Psi^t(\rho_{x,N})}(s_j)$ (see (47)) by a “bin size” $(s_{j+1} - s_{j-1})/2$ determined from the eigenvalue spacing (with appropriate modification at the endpoints). The results in Fig. 8 show rapid convergence to the true signal, manifested by an approximately five-fold increase of the probability density around the true signal with each increment of N . It is noteworthy that a modest number of qubits, e.g., $N = 3$ or 4, suffices to accurately track the true signal by the expectation $f_{t,N}(x)$. Of course, in an actual quantum computational environment there would be additional sampling errors, dependent on the number K of measurements used to estimate the mean. However, such errors would rapidly decrease with N , meaning that given sufficiently many qubits, the number of measurements needed to estimate the mean at the desired tolerance could be as small as $K = 1$.

V. CONCLUDING REMARKS

We have developed a framework for a quantum compiler, which translates the evolution of states and observables of a classical dynamical system into a quan-

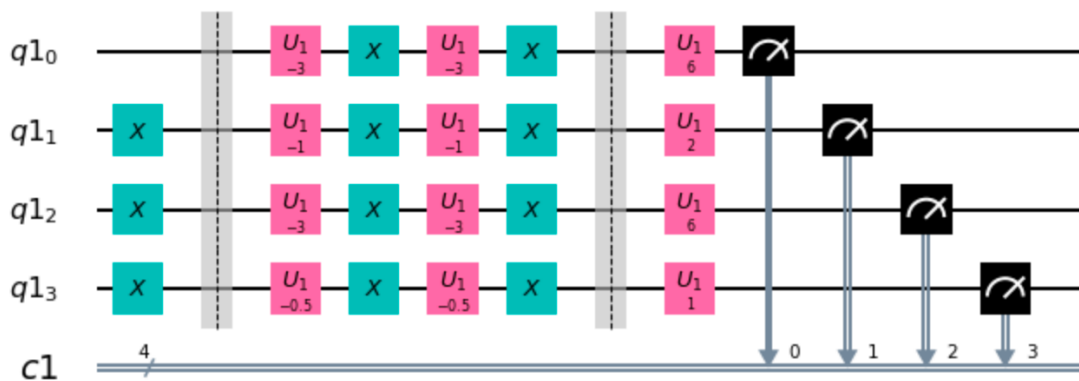


FIG. 6. Quantum circuit implementation in Qiskit for the 4-qubit approximation of an ergodic rotation on the 2-torus. The Pauli X gates to the left of the first barrier (vertical dashed line) are used to generate different input states on the quantum register. Between the barriers, global phase gates are set up for each of the 4 qubits. These are followed by rotation gates and the measurement section that stores the results on the classical register.

tum computation. The construction of the compiler was presented as a four-level procedure involving classical, classical statistical, quantum mechanical, and quantum computational representations of the system, the latter comprising of N qubits spanning a 2^N -dimensional Hilbert space. One of the mathematical underpinnings of our approach is reproducing kernel Hilbert space theory (RKHS), which is widely used in machine learning, but was employed here to construct quantum mechanical analogs of feature maps that behave consistently under classical function evaluation and quantum mechanical expectation. A further foundational ingredient is the operator-theoretic description of dynamical systems, which utilizes linear Koopman operators to characterize the action of a (nonlinear) dynamical system on observables.

We described how quantum compilation proceeds along two composite mappings, one taking state variables $x \mapsto \rho_x$ to density operators ρ_x , and one taking classical observables $f \mapsto \hat{S}$ to self-adjoint operators \hat{S} . A key aspect of the resulting quantum system is a tensor product factorization of its Hamiltonian in terms of Walsh operators, yielding quantum circuits of low connectivity. In particular, it was shown that for an ergodic dynamical system with finitely-generated pure point spectrum, the quantum compiler results in an N -qubit circuit with no cross-channel communication, enabling exponential scalability of the Hilbert space dimension at the expense of a linear increase of the required number of quantum gates.

We illustrated our approach with periodic and quasiperiodic dynamical systems on the circle and 2-torus, respectively, where many aspects of the quantum compiler are accessible analytically. Our numerical examples included a Qiskit implementation of a 4-qubit quantum channel representing quasiperiodic dynamics on a 2-torus, as well as simulated computation experiments demonstrating consistency between the predictions from the compiled quantum system and the true classical evolution.

The work presented in this paper should be considered as a first step, particularly given the simple dynamical systems that have been studied. Applications of the procedure to chaotic dynamical systems will invariably have to deal with continuous spectrum of the Koopman operator, generating quantum circuits of higher connectivity than for quasiperiodic dynamics. Studies in this direction are currently underway using RKHS-based spectral discretization approaches for Koopman operators [38], and will be reported elsewhere. Another avenue of future research is to develop data-driven formulations of the compiler, using kernel methods to build orthonormal bases in which to represent quantum mechanical states and observables [36]. A longer-term goal would be to explore applications of quantum mechanical methodologies to perform simulation and forecasting of real-world systems such as climate dynamics [39] and turbulent fluid flows [40].

ACKNOWLEDGMENTS

We wish to thank Sachin Bharadwaj for helpful discussions. D. Giannakis acknowledges support from NSF grants 1842538, DMS-1854383, and ONR MURI grant N00014-19-1-242. A. Ourmazd and J. Slawinska received support from NSF grant 1842538. The work of J. Schumacher is supported by the Deutsche Forschungsgemeinschaft and by the project “DeepTurb – Deep Learning in and of Turbulence” funded by the Carl Zeiss Foundation (Germany).

Appendix A: Injectivity of the quantum mechanical representation of classical observables

In this appendix, we verify the assertion made in Section III B 1 that the map $T : \mathcal{H} \rightarrow B(\mathcal{H})$ is injective on

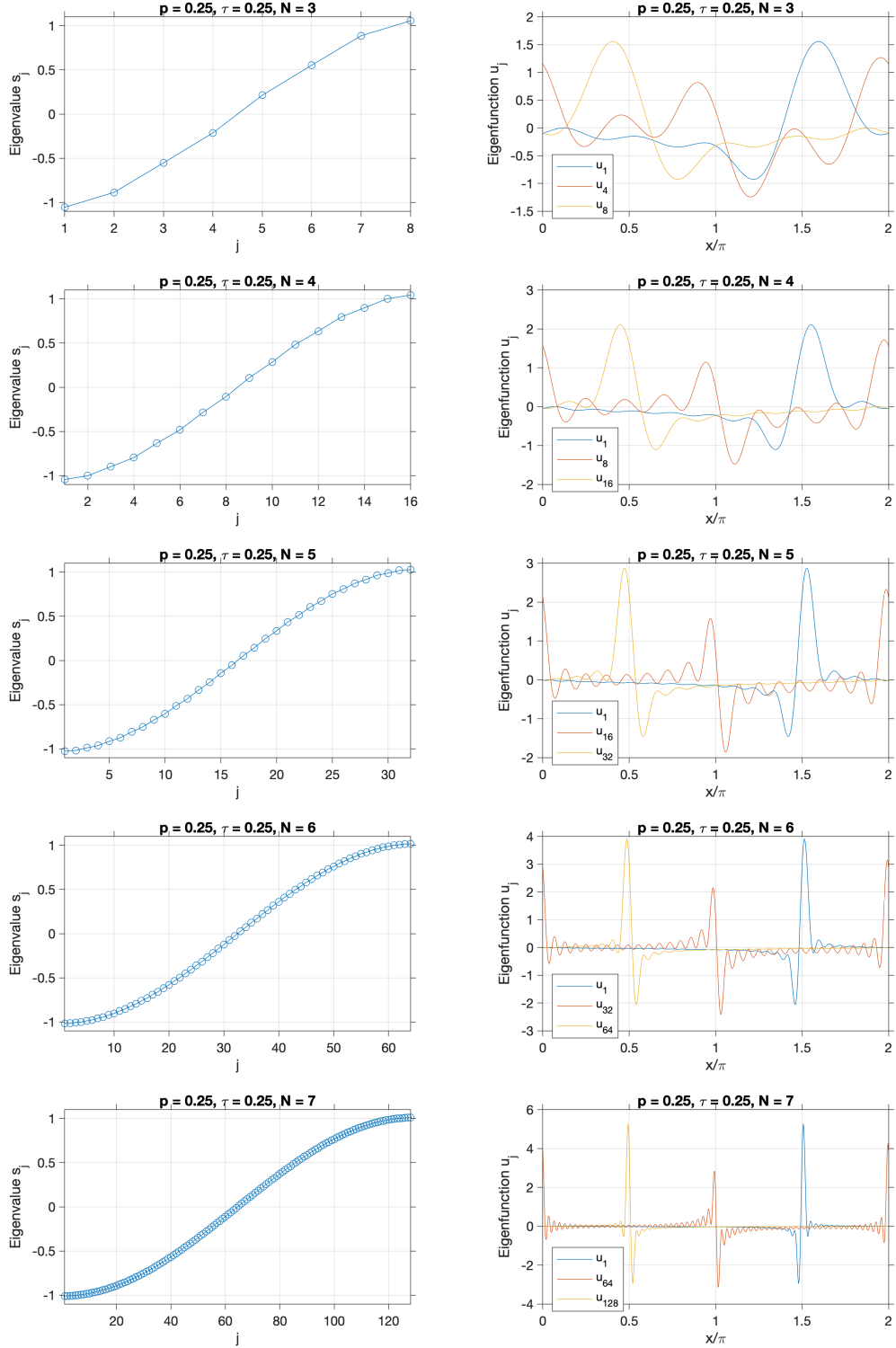


FIG. 7. Eigenvalues s_j (left-hand column) and representative eigenfunctions u_j (right-hand column) of the self-adjoint operators $S_{f,N}$ representing the classical observable $f(x) = \sin x$ for qubit number $N = 4, \dots, 8$. The RKHA parameters p and τ are set to the same values as in Figs. 4(a) and 5. Notice that as N increases the spectra of $S_{f,N}$ provide an increasingly dense sampling of the range of values of f , and the eigenfunctions $u_j(x)$ become increasingly localized around values of x for which $f(x) \approx a_j$.

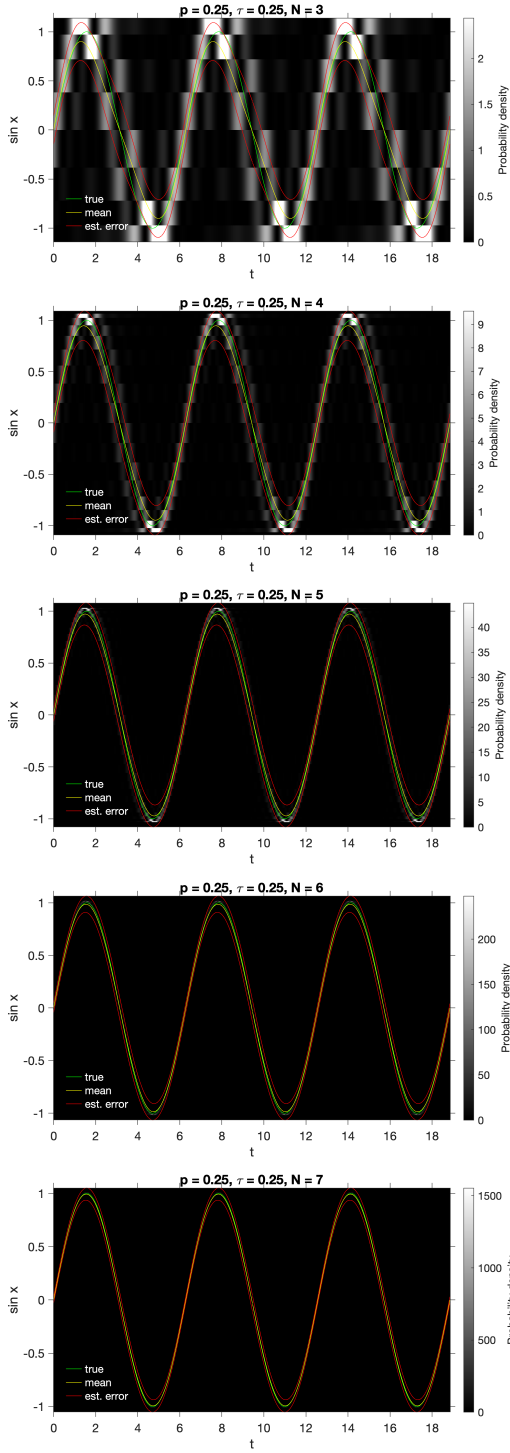


FIG. 8. Simulated prediction experiments of the observable $f(x) = \sin x$ of a circle rotation with frequency $\alpha = 1$, using the quantum systems from Fig. 7. Cyan and green lines show the true signal $f_t(x) = \sin(x + \alpha t)$ and quantum mechanical expectation value $f_{t,N}(x)$ for the initial condition $x = 0$. Red lines show estimated errors obtained from the square root of the expectation value of the quantum mechanical observable $(S_{f,N} - f_{t,N}(x))^2$. Colors correspond to the quantum probability density obtained from the spectral resolution of $S_{f,N}$ via (47).

\mathcal{H}_{sa} . For that, it is enough to show that if $Tf = 0$ for $f \in \mathcal{H}_{\text{sa}}$, then $f = 0$. By definition of T , $Tf = 0$ implies that $\pi f = -(\pi f)^*$, or, equivalently

$$\langle \psi_i, f \psi_j \rangle_{\mathcal{H}} = -\langle f \psi_i, \psi_j \rangle_{\mathcal{H}}.$$

Expanding $f = \sum_{l \in \mathbb{Z}^d} \tilde{f}_l \psi_l$, and setting $i = 0$ in the above, we get

$$\tilde{f}_j^* = -c_{j,-j} \tilde{f}_{-j}.$$

However, because f is real, we have $\tilde{f}_j^* = \tilde{f}_{-j}$, and since $c_{j,-j}$ is nonzero we conclude that $\tilde{f}_j = 0$, and thus $f = 0$.

Appendix B: Calculation of the discrete Walsh transform

Here, we lay out the calculation of the discrete Walsh transform for the special case, that Rademacher functions $R_l = w_{2^l}$ are used only. By (20), h splits as

$$h(m/2^N) = \alpha_1 j_1 + \alpha_2 j_2 + \dots + \alpha_d j_d, \quad (\text{B1})$$

where j_1, \dots, j_d are integers in the set J_1 , defined uniquely by the property that the concatenated binary strings $\eta(j_1), \dots, \eta(j_d)$ give the dyadic decomposition of $m/2^N$,

$$\gamma(m/2^N) = (\eta(j_1), \dots, \eta(j_d)).$$

In particular, using (42), and setting $m_l = \zeta(j_l)$, we get the following expression

$$\begin{aligned} & (R_0(m/2^N), \dots, R_{N-1}(m/2^N)) \\ &= (\eta(j_1), \eta(j_2), \dots, \eta(j_d)) \\ &= (\gamma(m_1/2^{N/d}), \gamma(m_2/2^{N/d}), \dots, \gamma(m_d/2^{N/d})) \\ &= (R_0(m_1/2^{N/d}), \dots, R_{N/d-1}(m_1/2^{N/d}), \\ & \quad R_0(m_2/2^{N/d}), \dots, R_{N/d-1}(m_2/2^{N/d}), \dots, \\ & \quad R_0(m_d/2^{N/d}), \dots, R_{N/d-1}(m_d/2^{N/d})). \end{aligned}$$

The above implies that for each $i \in \{1, \dots, d\}$ and $l \in \{0, \dots, N-1\}$ we have

$$R_l(m/2^N) = R_{l-(i-1)N/d}(m_i/2^{N/d}), \quad (\text{B2})$$

for all $m \in \{0, \dots, 2^N - 1\}$. Observe now that for $j_i \in J_1$,

$$\begin{aligned}
j_i &= \begin{cases} m_i - 2^{N/d-1} & : 0 \leq m_i \leq 2^{N/d-1} - 1, \\ m_i - 2^{N/d-1} + 1 & : 2^{N/d-1} \leq m_i \leq 2^{N/d} - 1 \end{cases} \\
&= \sum_{l=0}^{N/d-1} (1 - R_l(m_i/2^{N/d}))2^{-l-2+N/d} + \frac{1 - R_0(m_i/2^{N/d})}{2} - 2^{N/d-1} \\
&= - \sum_{l=0}^{N/d-1} R_l(m_i/2^{N/d})2^{-l-2+N/d} - R_0(m_i/2^{N/d})/2 \\
&= \sum_{l=0}^{N/d-1} R_{l+(i-1)N/d}(m/2^N)2^{-l-2+N/d} - R_{(i-1)N/d}(m/2^N)/2.
\end{aligned}$$

We used Eq. (B2) to obtain the last line of this expression. Substituting the above in (B1), we conclude that for a quasiperiodic system, the spectral function h is express-

ible as a linear combination of Rademacher functions (as opposed to more general Walsh functions). Specifically, we get now

$$h(m/2^N) = \sum_{i=1}^d \alpha_i \left(\sum_{l=0}^{N/d-1} R_{l+(i-1)N/d}(m/2^N)2^{-l-2+N/d} - \frac{1}{2}R_{(i-1)N/d}(m/2^N) \right).$$

This simplification has consequences for the expansion generator $V = iH$ or Hamiltonian H which are discussed

in the main text and lead to an implementation on the quantum computer that does not create additional entanglement.

-
- [1] R. P. Feynman, *Int. J. Theor. Phys.* **21**, 467 (1982).
 - [2] S. Lloyd, *Science* **273**, 1073 (1996).
 - [3] D. W. Berry, G. Ahokas, R. Cleve, and B. C. Sanders, *Commun. Math. Phys.* **270**, 359 (2007).
 - [4] S. Barnett, *Quantum Information*, Oxford Master Series in Atomic, Optical and Laser Physics (Oxford University Press, Oxford, UK, 2009).
 - [5] M. A. Nielsen and I. L. Chuang, *Quantum Computation and Quantum Information* (Cambridge University Press, Cambridge, UK, 2010).
 - [6] J. Preskill, *Quantum* **2**, 79 (2018).
 - [7] L. K. Grover, *Am. J. Phys.* **69**, 769 (2001).
 - [8] F. Arute, K. Arya, R. Babbush, D. Bacon, and et al., *Nature* **574**, 505 (2019).
 - [9] G. Benenti, G. Casati, S. Montangero, and D. L. Shepelyansky, *Phys. Rev. Lett.* **87**, 227901 (2001).
 - [10] S. K. Leyton and T. J. Osborne, arXiv:0812.4423 (2008).
 - [11] D. Giannakis, *Phys. Rev. E* **100**, 032207 (2019).
 - [12] I. Joseph, *Phys. Rev. Research* **2**, 043102 (2020).
 - [13] S. Bharadwaj and K. R. Sreenivasan, *Pramana* **123**, in press (2020).
 - [14] F. Gaitan, *npj Quantum Inf.* **6**, 61 (2020).
 - [15] M. Lubasch, J. Joo, P. Moinier, M. Kiffner, and D. Jaksch, *Phys. Rev. A* **101**, 010301(R) (2020).
 - [16] V. Baladi, *Positive transfer operators and decay of correlations*, Advanced Series in Nonlinear Dynamics, Vol. 16 (World scientific, Singapore, 2000).
 - [17] T. Eisner, B. Farkas, M. Haase, and R. Nagel, *Operator Theoretic Aspects of Ergodic Theory*, Graduate Texts in Mathematics, Vol. 272 (Springer, 2015).
 - [18] J. C. Ferreira and V. A. Menegatto, *Ann. Funct. Anal.* **4**, 64 (2013).
 - [19] V. I. Paulsen and M. Raghupathi, *An Introduction to the Theory of Reproducing Kernel Hilbert Spaces*, Cambridge Studies in Advanced Mathematics, Vol. 152 (Cambridge University Press, Cambridge, 2016).
 - [20] J. Biamonte, P. Wittek, N. Pancotti, N. Wiebe, and S. Lloyd, *Nature* **549**, 195 (2017).
 - [21] C. Ciliberto, M. Herbster, A. D. Ialongo, M. Pontil, A. Rocchetto, S. Severini, and L. Wossnig, *Proc. R. Soc. A* **474**, 20170551 (2018).
 - [22] M. Schuld and N. Killoran, *Phys. Rev. Lett.* **122**, 040504 (2019).
 - [23] <https://qiskit.org/textbook/preface.html> (2020).
 - [24] C. J. Wood, <https://medium.com/qiskit> (2018).
 - [25] B. O. Koopman, *Proc. Natl. Acad. Sci. USA* **17**, 315 (1931).
 - [26] B. O. Koopman and J. von Neumann, *Proc. Natl. Acad.*

- Sci. USA **18**, 255 (1931).
- [27] B. Schölkopf, A. Smola, and K. Müller, *Neural Comput.* **10**, 1299 (1998).
- [28] A. Peres, *Quantum Theory: Concepts and Methods*, edited by A. Van der Merwe, *Fundamental Theories of Physics*, Vol. 72 (Kluwer Academic Publishers, New York, 2002).
- [29] M. Budisić, R. Mohr, and I. Mezić, *Chaos* **22**, 047510 (2012).
- [30] M. H. Stone, *Ann. Math* **33**, 643 (1932).
- [31] F. Cucker and S. Smale, *Bull. Amer. Math. Soc.* **39**, 1 (2001).
- [32] S. Das and D. Giannakis, “Reproducing kernel Hilbert algebras on compact Lie groups,” (2019).
- [33] W. Rudin, *Fourier Analysis on Groups* (Dover Publications, Mineola, 2017).
- [34] S. Das and D. Giannakis, *Appl. Comput. Harmon. Anal.* **49**, 573 (2020).
- [35] D. Giannakis, “Quantum dynamics of the classical harmonic oscillator,” (2019).
- [36] D. Giannakis, *Appl. Comput. Harmon. Anal.* **62**, 338 (2019).
- [37] J. Welch, D. Greenbaum, S. Mostame, and A. Aspuru-Guzik, *New J. Phys.* **16**, 033040 (2014).
- [38] S. Das, D. Giannakis, and J. Slawinska, “Reproducing kernel Hilbert space quantification of unitary evolution groups,” (2020), in minor revision, 1808.01515.
- [39] J. Slawinska, A. Ourmazd, and D. Giannakis, in *Workshop on “Climate Change: How Can AI Help?”*, *36th International Conference on Machine Learning (ICML)* (Long Beach, California, 2019).
- [40] D. Giannakis, A. Kolchinskaya, D. Krasnov, and J. Schumacher, *J. Fluid Mech.* **847**, 735 (2018).